NTNU – Trondheim
Norwegian University of
Science and Technology

Experimental Testing of Initial Hook Load During Tripping in Horizontal Well

Robin Dragstmo Andersen

Petroleum Geoscience and Engineering
Submission date: June 2015
Supervisor: Pål Skalle, IPT

Norwegian University of Science and Technology
Department of Petroleum Engineering and Applied Geophysics

Acknowledgement

This thesis is the result of long hours in the lab at the Department of Petroleum Engineering and Applied Geophysics at NTNU. The work could not have been done without the help and support of several individuals.

First I would like to thank my supervisor and Associated Professor at NTNU, Pål Skalle. He helped me with a lot of enthusiasm and motivation.

I would also like to thank the lab technicians, Håkon Myhren for the countless hours he spent building and setting up my experiment, and Åge Sivertsen for making all the electronic components work.

My thanks also goes out to my father, who has given me support not only through this work, but through all my studies.

Trondheim, June 2015

_____

Robin Dragstmo Andersen

Abstract

One of the major problems in drilling operations occur during tripping out of the well. Inside the well there are often restrictions making it difficult or impossible to pull out the drill string including its bottom hole assembly, especially in extended reach wells. The consequences of not recognizing the problem in time could be a deformed drill string, or worse, a severed drill string. By understanding the causes of the problems it becomes easier to deal with them. The focus in the present work was on the initial hook load peak showing up during tripping operations in horizontal wells. The major part of the work was put into the building of a custom designed laboratory environment that simulated tripping operations. The work was based on previous work on the subject. The hook load was measured by tension meters and recorded with a custom designed program created in a computer software; LabView. The hook load was also modelled mathematically to be able to compare theoretical results with the laboratory results as well as with field data.

The experiments were performed with variables like drill string elasticity, velocity and wellbore wall surface. The laboratory design was also created for future development to better understand the hook load during tripping operations.

The model lacked initial elastic condition data, which made it impossible to properly simulate the laboratory tripping operation. The final custom designed program (LabView) produced results from the experimental runs that were much like the acquired field data.

Sammendrag

En av de største problemene i boreoperasjoner skjer under tripping ut av brønnen. I brønnen så er det ofte hindringer som gjør det vanskelig eller umulig å dra ut borestrengen inkludert bottom-hole-assembly, spesielt i extended-reachbrønner. Konsekvensene av å ikke legge merke til problemet i tide kan være en deformert borestreng, eller værre, en frarevet borestreng. Ved å forstå årsakene til disse problemene så blir de enklere å håntere. Fokuset i dette arbeidet var på den initielle hook-load-peaken under trippingoperasjoner i horisontale brønner. En stor del av arbeidet ble lagt i byggingen av et spesialdesigned laboratorie miljø, som simulerte trippingoperasjoner. Arbeidet var basert på tidligere arbeid om det samme temaet. Hook-loaden ble målt av strekkmålere og ble prosessert av et spesialdesignet program som ble laga i et komputer-software; LabView. Hook-loaden ble også modellert matematisk for å kunne sammenligne teoretiske resultater med laboratorieresultater så vel som med felt data.

Eksperimentet ble utført med variabler som borestrengelastisitet, hastighet og brønnveggoverflate. Laboratoriedesignen ble også skapt for fremtidig utvikling for å bedre forstå hook-loaden under trippingoperasjoner.

Modellen manglet elastiske initialbetingelser, som gjorde det umulig å ordentlig simulere laboratorietrippingoperasjonen. Det endelige spesialdesignet programmet (LabView) produserte resultater fra eksperimentet som ble veldig likt de tilegnede feltdataene.

Table of Contents

Acknowledgement i

Abstract ii

Sammendrag iii

List of Figures vi

List of Tables viii

1. Introduction 1

2. Forces Acting on the Drill String 3

   2.1. Drilling Rig Hoisting System 3

   2.2. Mechanical Friction on the Drill String 4

      2.2.1. Dry Friction 5

      2.2.2. Lubricated Friction 6

      2.2.3. Coefficient of Friction in Static and Dynamic Conditions 7

   2.3. Elastic Behavior 9

      2.3.1. Hook's Law 9

3. Previous Relevant Knowledge on Modeling and Experimental Investigation of Hook Load 10

   3.1. Modeling of Hook Load 10

   3.2. Experimental Investigation on Hook Load 11

   3.3. Normal Behavior 11

   3.4. Poor Bore Hole Conditions 14

4. Mathematical Model of Peak Behavior 16

   4.1. Supportive Knowledge of the Models 16

   4.2. The Model of the Dynamic Peak 18

5. Experimental Investigation of HKL 19

   5.1. Design of Lab Experiment 20

   5.2. The Schedule of Erecting the Rig 22

5.3. Procurement of Material and Equipment 25
5.3.1. Equipment Specification 26
5.3.2. Electronics 32
5.3.3. LabView 33
5.4. Test Matrix 35
5.4.1. Trial Runs and Quality Checking 37
6. Experimental Results 43
6.1.1. Familiarizing with the Results 43
6.1.2. Result Evaluation 46
7. Discussion 58
7.1. Quality of the Model 58
7.2. Quality of the Experiment 58
7.3. Future Work 60
8. Conclusion 62
9. Nomenclature 63
10. References 66
11. Appendix 67

List of Figures

Figure 1: Drilling Rig Hoisting System (Engineering, 2015) 4
Figure 2: Friction Force 6
Figure 3: Static to Dynamic Friction 8
Figure 4: Normal Tripping Conditions in Vertical Well (Cordoso et al., 1995) 12
Figure 5: Field Data Whole Drill Pipe Tripping Operation (Statoil, 2007) 13
Figure 6: Field Data Several Stands Tripping Operation (Statoil, 2007) 13
Figure 7: Field Data One Stand Tripping Operations (Statoil, 2007) 14
Figure 8: The Mass-Spring System. Above at initial time, below at time step t (Glomstad, 2012) 17
Figure 9: Matlab; Simple HKL Model of Experiment 18
Figure 10: Set Up Design in 3D Perspective 19
Figure 11: Work Space Schematics 20
Figure 12: Design Overview of Hook Load Rig 21
Figure 13: Detailed Equipment Design 26
Figure 14: Winch and Motor; Simulating the Draw Works on a Drilling Rig 26
Figure 15: Metal Block Simulating the BHA 27
Figure 16: Springs for Drill String Elastic Behavior 29
Figure 17: Sheaves with Dynamo 30
Figure 18: Electronic Schematics for Hook Load Rig (Designed by this author in Microsoft Visio) 32
Figure 19: LabView Front Panel shows the following 6 items: Stop button (upper left button), TM2000 (upper left chart), TM200 (lower left chart), Wire Velocity (lower right chart and bottom meter) and Voltage ALL (upper right chart). 33
Figure 20: LabView Block Diagram; the signal flow (designed in LabView by this author) 34
Figure 21: Disturbed Signals 39
Figure 22: Disturbed Signals with Coiled Wires 39
Figure 23: Final Block Diagram; Same signal flow but with higher sampling rate and new filters (designed in LabView by this author) 40
Figure 24: Front Panel with New Filters 41
Figure 25: Flow Chart of Running Procedure 42
Figure 26: HKL in TM2000 (left chart) and in TM200 (right chart) 43

Figure 27: Velocities; Low (upper left), High (upper right), Super High (lower left) and Ultra High (lower right) 44
Figure 28: Raw data charts with high sampling rate program (upper left and right) and low sampling program (lower left and right) of low (left charts) and high velocity (right charts). 45
Figure 29: HKL of TM2000 and TM200 from first program without filters (upper left and right) and second program with filters (lower left and right). 46
Figure 30: HKL on metal surface with medium low spring strength. Run velocity increasing from low to ultra high in the following order; top, center left, center right, lower left, lower right. 47
Figure 31: HKL on metal surface at high velocity. Spring strength increasing from low to high in the following order; top, center left, center right, lower left, lower right. 49
Figure 32: HKL on dry sand with two spring strengths and two velocities. The charts show the following: Medium low spring strength, low velocity (upper left) and high velocity (upper right); High spring strength, low velocity (lower left) and high velocity (lower right). 50
Figure 33: HKL on water-wet cuttings with two spring strengths and two velocities. The charts show the following: Medium low spring strength, low velocity (upper left) and high velocity (upper right); High spring strength, low velocity (lower left) and high velocity (lower right). 51
Figure 34: HKL on metal (upper charts), dry cuttings (center charts) and water-wet cuttings (lower charts). Both medium low spring strength (left charts) and high spring strength (right charts) ran with low velocity. 52
Figure 35: HKL on metal (upper charts), dry cuttings (center charts) and water-wet cuttings (lower charts). Both medium low spring strength (left charts) and high spring strength (right charts) ran with high velocity. 53
Figure 36: The stabilized “constant” HKL signal vs. type of friction and vs. spring strength at constant velocity (high) 54
Figure 37: Initial HKL vs. velocity at constant spring strength (high) 55

List of Tables

Table 1: Action Plan During Building of the Rig 24
Table 2: Procurement List. Status as of April 15th 25
Table 3: Specs for 5 Different Extension Springs 28
Table 4: Calibrated Wire Velocity 30
Table 5: Voltage and Velocity Calibration 31
Table 6: Activity in the Test Matrix for Qualifying the Experimental Rig 36
Table 7: Initial Test Matrix, with maximum 48 # of runs 36
Table 8: Final Test Matrix, with maximum 45 # of runs 37
Table 9: Static Friction Factor vs. Type of Surface 55

1. Introduction

Over the past years drilling for petroleum has become more challenging. In order to produce oil and gas, the wells have become deeper and more complex, requiring better techniques and more advanced technology. These types of wells are not the typical straight and vertical, but curved in the horizontal as well as in the vertical plane. The bottom hole assembly (BHA) is commonly retrieved several times during a drilling operation of a single well, and are referred to as tripping operations. Many complications occur when tripping in these complex wells.

When pulling out of hole the most common problem is stuck pipe, which can result in severing or permanently deforming the drill string if pulled too hard. Stuck situations happen due to unexpected restrictions in the wellbore. The hook load (HKL) is the measurement of the tensional force of the drill string, which is suspended from the hook of the traveling block. The reason for measuring the HKL is to prevent damaged equipment and non-productive time (NPT), as lost time gets very costly.

High string stress is a common reoccurring phenomenon in the initial phase of pulling out the drill string in horizontal wellbores, especially in extended reach drilling (ERD). The drill string is firstly stretched in the vertical, friction free section, and gradually stretched and set in motion further away as the tensional forces become higher than the static frictional forces. Finally the BHA is brought out of its static state, which, due to high static friction forces results in a sudden forward jerk. This jerking action can be observed at the surface hook load. The initial hook load peak is thought to be followed by a reactive oscillating compressional wave before leveling off at a constant hook load, lower than the initial peak.

The goal of the work is to gain a sufficient understanding of the string pulling operation to be able to evaluate whether or not the operation is critical, and eventually, whether or not any counter measures can be taken to mitigate or overcome the challenges. The goal will be achieved by collecting and extending the basic knowledge of initial hook load tension.

A theoretical mathematical model of the physics involved will be created. The model will be compared to experimentally produced data from a simulated environment. The results of these tests will then be analyzed and compared with a third source of relevant data; documented field data. Having three independent sources will help verify the credibility of the experimental results.

The initial peak, observed in the hook load, will be the main focus, as this is one of the critical points of a tripping operation if performed too abruptly. The hypothesis is that with the right experimental equipment a hook load-peak could be created that would simulate the field operation hook load.

2. Forces Acting on the Drill String

The HKL is defined as the actual weight of the drill string including the BHA. It measures the force pulling down from the hook of the traveling block, which holds the top end of the drill string. The HKL is a measurement in units of weight (N). The weight is affected by several factors, such as friction, gravity, buoyancy and gravity (PetroWiki, 2013). There are also other factors that play both minor and major roles in the HKL. A minor role could be mud circulation (drag force) or well temperature. A major role could be cuttings, ledges, swelling etc. These factors create both normal and abnormal HKL.

The reason for measuring the HKL is to be able to know the weight on bit (WOB) when drilling, and to know how much tension is put on the drill pipe when tripping out. Abnormal HKL measurements could mean potential problems, like stuck pipe. Damaged tools and stuck pipe is a major cause of NPT. Predicting and measuring the HKL can mitigate the overall NPT, which can consumes up to 35 % of the operation costs (Sjøbrend, 2014).

2.1. Drilling Rig Hoisting System

The drilling rig hoisting system is what operates the drill string. The hoisting system uses a large pulley system that lowers and raises tools in and out of the well. The basic components of the system are shown in Figure 1. The drilling hook, attached to the traveling block, hooks on to and suspends the drill pipe. The elevators clamp on to the drill string once it is on the hook. The draw works has a drum that uses an electric motor and gear system to reel in a wire rope called the drilling line. The draw works uses a clutch and gear system when spooling in the wire (pulling out of hole), and a brake when running into the hole. From the draw works the wire rope is reeved over a set of sheaves called the crown block. The crown block is located at the top of the derrick. The wire then goes from the crown block and reeves over the sheaves of the traveling block. When the draw works spool in or out the traveling block moves up or down. The wire then goes over to the dead line anchor and reserve drum from the crown block. This end of the wire is called the dead line because it normally does not move. The HKL is usually measured in the dead line, from the anchor. The reserve drum is used in the case of an emergency and the draw works stops working (Engineering, 2015).

The load on the fast line and dead line can be determined by the number of lines N, between the two blocks in the pulley system, and the weight hanging from the hook as seen in Eq. (1).

$$W = F_{dl} \cdot N \quad (1)$$

The tension in the deadline is measured as F_{dl}, and the hook load is the weight suspended from the traveling block. In this formula the friction in the sheaves is neglected (Aadnoy et al., 2010).

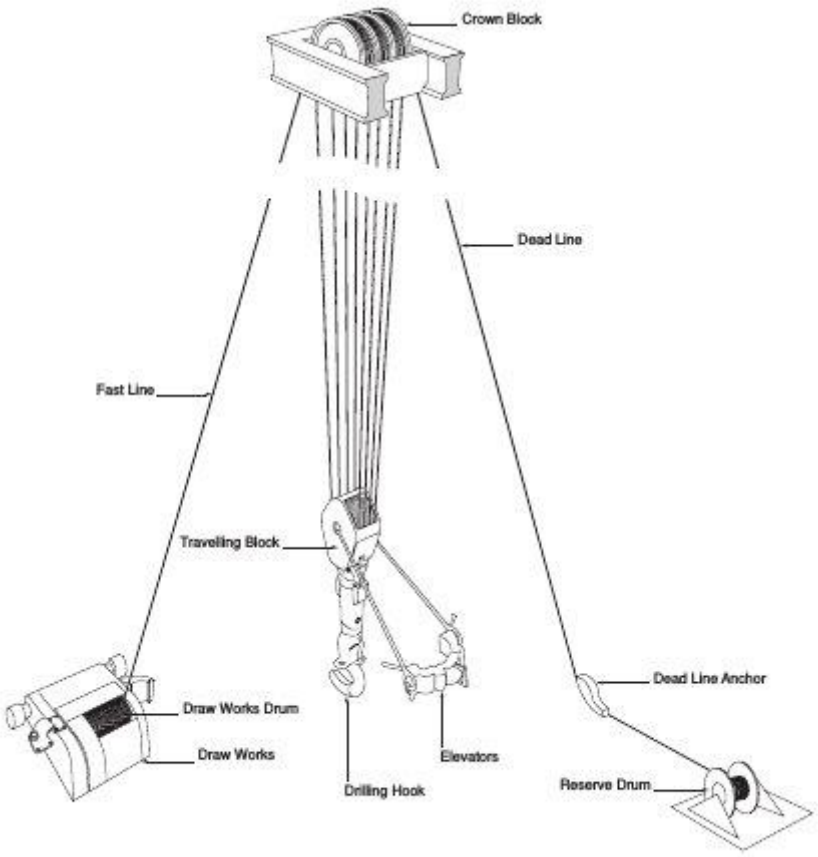

Figure 1: Drilling Rig Hoisting System (Engineering, 2015)

The pulley system also requires pulling the wire N times the distance the traveling block moves. This system makes the drilling operation much more effective in lifting heavy weight. The number of sheaves used depends on the weight of the load.

2.2. Mechanical Friction on the Drill String

The friction created in the wellbore affects the HKL considerably, both when going into the well and when going out. Friction is the force resisting relative motion (Wikipedia, 2015). It

always works against the moving direction. So when the drill string goes into the well the measured HKL decreases compared to when the drill string is in a neutral and static position (not in tension and not moving), while the measured HKL increases when pulling out of hole (POOH).

In ERD wells the problem of friction only increases. This is because of larger surface area contact between the bore hole walls and drill string.

Friction acts in different ways depending on the conditions and mediums involved. The different types of friction experienced in drilling operations are (Kristensen, 2013):

- Dry friction
  - Between two solid surfaces
  - Static friction and dynamic friction
- Lubricated friction
  - Two solid surfaces separated by a thin fluid layer
- Skin friction
  - Moving a solid material through fluid
- Fluid friction
  - Between layers within a viscous fluid
- Internal friction
  - Related to material stiffness and deformation

The main focus in the experimental investigation was dry friction and lubricated friction, and therefore they receive more attention.

2.2.1. Dry Friction

Coulomb friction is the simplest form of expressing friction forces. The formula expressing Coulomb friction is as follows in Eq. (2).

$$F_f \leq \mu \cdot F_N \tag{2}$$

This equation expresses static friction force. The friction force between an object and a surface is at all time less than or equal to the normal force of the object times the friction factor, also known as the coefficient of friction (CoF). This is the static friction factor, as the friction factor changes when the object is in motion. If the forces acting upon the object surpass the friction force, the object starts moving. A typical illustration of basic friction forces is presented in Figure 2 bellow.

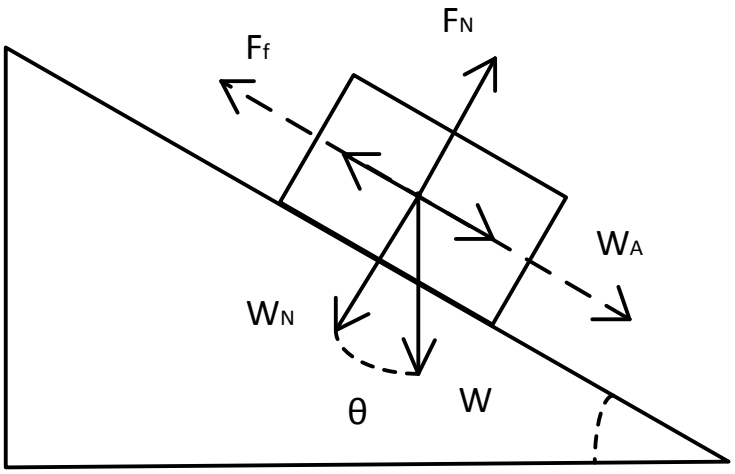

Figure 2: Friction Force

When the object is static the friction force is expressed as:

$$F_f = W_A \leq \mu_s \cdot F_N \tag{3}$$

$$W_A = W \cdot sin\theta \tag{4}$$

$$F_N = W \cdot cos\theta \tag{5}$$

In a dynamic situation, with the object being pulled up the angle, the friction factor changes to a dynamic constant, and the angle force F_A needed to move the object would be expressed as following:

$$F_A = W_A + \mu_d \cdot F_N \tag{6}$$

The friction force changes direction, and goes against the direction of motion.

2.2.2. Lubricated Friction

Lubrication is a process technique that reduces the friction between surfaces by interposing a substance with friction reducing attributes. Common lubricant groups are: base oil, biolubricants, synthetic oil, solid lubricants and aqueous lubricants. A basic lubricant, even though not always the most effective, is water. Water is a very common lubricant in drilling

operations, especially when spudding a new offshore well without a riser. The drilling fluids in general act as a lubricant, and the most common one to use, for environmental reasons, is water based mud (WBM), even though oil based mud (OBM) is not uncommon. Both water and drilling mud were chosen lubricants for the experimental testing.

In drilling operations the muds lubrication characteristics reduce the friction forces acting on the drill string and BHA when running in hole (RIH) or tripping out, but more importantly for POOH. Previous laboratory experiments showed that the CoF's are affected by mud quality, mudcake and lubricant additives (Maidla and Wojtanowicz, 1990). The mudcake creates a barrier on the bore hole walls, which reduces the CoF. OBM proves to be more effective than WBM in reducing the friction. Other laboratory experiments done showed that by adding small polymer micro beads in the drilling fluid, the WBM could also reduce the friction factor, by as much as 40 % (Kristensen, 2013).

2.2.3. Coefficient of Friction in Static and Dynamic Conditions

The CoF changes from a static state to a dynamic state, but are considered constants in each state. It is the scalar that predicts the required force needed in order to move the drill string.

Different materials have different surface roughness, and so the friction factor depends on the roughness and combination of the materials that interact. The friction factor can be expressed as:

$$\mu = \frac{F_f}{F_N} \tag{7}$$

Because the CoF changes from static to dynamic condition the required force applied to the object also changes. Assuming a perfect scenario with no oscillating behavior and no elastic behavior in the drill string, the force - time plot would look very much like Figure 3.

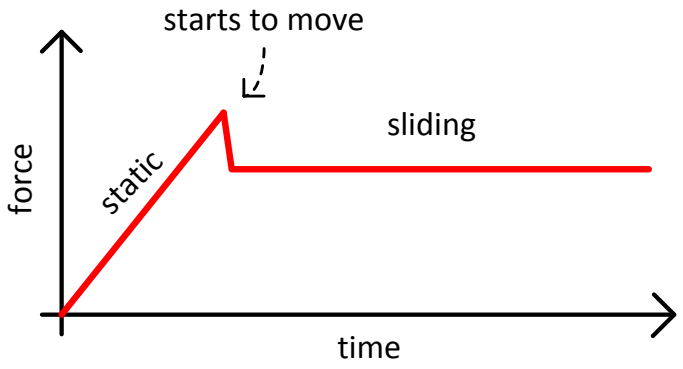

Figure 3: Static to Dynamic Friction

This is exactly what the experimental investigation was about, to show the changing in the required force when moving the drill string from the static to the dynamic state. Figure 3 shows that the friction coefficient changes when the drill string is moving. This shows the following:

$$\mu_s > \mu_d \tag{8}$$

Other contributors to the friction model besides the surface roughness of the drill pipe and wellbore walls are (Sjøbrend, 2014):

- Pipe stiffness
- Viscous drag (fluid resistance)
- Mud lubrication
- Formation rock type
- Contact points
- Cutting bed
- Pore pressure

Some of the typical obstructions that play a part in the HKL model are expanded upon in section 3.4 Poor Bore Hole Conditions. The HKL model is a more advanced version of the friction model.

2.3. Elastic Behavior

In drilling operations the elastic behavior mainly occurs in the drill string. Elasticity is a materials ability to return to its original form after a deformation. When the drill string runs into the well it compresses due to the forces acting against it. When the BHA is tripped out of the hole, the drill string is forced to stretch. The longer the length of the drill string, the longer it stretches. If the acting forces are too strong for the material and structure of the drill string it buckles under compression and severs under extension. This deforms the structure of the drill string permanently, compromising and weakening its characteristics. The parameters for the elastic and permanent deformation can be expressed as (Kristensen, 2013):

$$\sigma = \frac{F}{A_{cs}} \tag{9}$$

$$\varepsilon = \frac{\Delta L}{L} \tag{10}$$

$$E = \frac{\sigma}{\varepsilon} \tag{11}$$

The stress is expressed as σ, the force as F and A_{cs} is the cross section area. Strain ε is defined as the deformation ΔL over the initial length L. E expresses Young's Modulus.

For the purpose of running in and tripping out of hole, it becomes very important to know the HKL in regards to the elasticity of the drill string for a couple of reasons. One reason is that a permanent deformation of the drill string can be very costly and lead to NPT. By knowing the yield stress of the equipment the operator will know the maximum allowed HKL without damaging it. The second reason is to understand the oscillating behavior of the drill string once the BHA starts moving. Different types of oscillations and abnormal HKL can mean different types of obstructions (Cordoso et al., 1995).

2.3.1. Hook's Law

In order to simulate the drill string elasticity, different springs are used in the experimental investigation. Extension springs have a great ability to stretch and return to its original form. Hook's law expresses the condition of a spring under certain forces. The force acting on the spring is expressed as:

$$F = k \cdot \Delta x \tag{12}$$

3. Previous Relevant Knowledge on Modeling and Experimental Investigation of Hook Load

The topic of HKL has not received a lot of attention in the research field, which can be a bit surprising considering that one of the major reasons for NPT in drilling operations is stuck pipe during tripping operations.

In 2011, with support from NFR and Det Norske, a hook load rig with a flow loop was built at NTNU. This started a number of experiments that has investigated different aspects of the HKL in tripping operations.

3.1. Modeling of Hook Load

The true HKL and line tension under dynamic conditions were investigated in 1993 in order to better predict the HKL in the field (Luke and Juvkam-Wold, 1993). Focusing on the hoisting system and the calculations done for HKL, they proved that the methods that were used to predict the HKL were off by as much as 19 %. They also concluded that the error increased as the number of lines between the blocks increased (Luke and Juvkam-Wold, 1993).

Another paper was written in 1995 on problem detecting during tripping operations in horizontal and directional wells (Cordoso et al., 1995). Through field analysis they created tripping curves that represented different well conditions. The curves showed how the HKL changed from a normal situation with no obstructions (see Figure 4) to curves with all kinds of abnormal conditions. The investigation gave a great insight in the importance of reading the HKL measurements and analyzing them to avoid damaging the equipment. Further they concluded that "the field case study supports the use of the Type Curve Matching Technique, that includes 'Hook Load Data Analysis' and the 'Pseudo Friction Factor Analysis'" (Cordoso et al., 1995).

At NTNU the mass-spring system was presented in an attempt to make a mathematical model of the behavior of the drill string during a tripping operation (Mme, 2012). The model describes the HKL by modeling a mass-spring system with the elastic behavior of the springs, and including the friction force through the mass and fluid drag. Kristensen (2013) worked on simulating the tripping operation using the mass-spring model. He found it too difficult to further develop the model due to lack of expertise and experience, and went over to working

on an alternative model. The alternative model was less successful in modeling field data HKL.

Bjerke (2013) analyses field data of tripping operations. From having studied papers such as "Problem Detection During Tripping Operations in Horizontal and Directional Wells" (Cordoso et al., 1995), she analyses actual field data by looking at HKL data from different wells. She discussed the causes for the restrictions in order to advance the understanding of HKL reading.

3.2. Experimental Investigation on Hook Load

Glomstad (2012), another Master's student at NTNU continued the work by setting up an experiment that simulated a tripping operation. She pulled a BHA through an annulus (pipe) with a circulating drilling fluid. During the tripping she measured wire tension, pulling velocity, fluid circulation and pipe expansion change. Sjøbrend (2014), two years later, improved the rig by creating it sturdier so that it could withstand higher forces. This was done by lowering the rig closer to the ground and bolting it to the concrete floor. He also built a new and stronger winch. He experimented with different types of BHAs while circulating cuttings in order to simulate different types of obstructions in the well during the tripping. His results were relatable to some of the curves developed in the paper by Cordoso et al. (1995). He also compared some of the results with the recognition model of Bjerke (2013).

3.3. Normal Behavior

There is no such thing as perfectly ideal conditions in the field. The closest to an ideal tripping operation is when there are no obstructions in the well, and only the friction forces are acting on the drill string. A paper on problem detecting during tripping operations expresses the normal conditions and called it a standard tripping type curve. Figure 4 shows the tripping of an entire stand in a vertical well, having used the Type Curve Matching Technique (Cordoso et al., 1995).

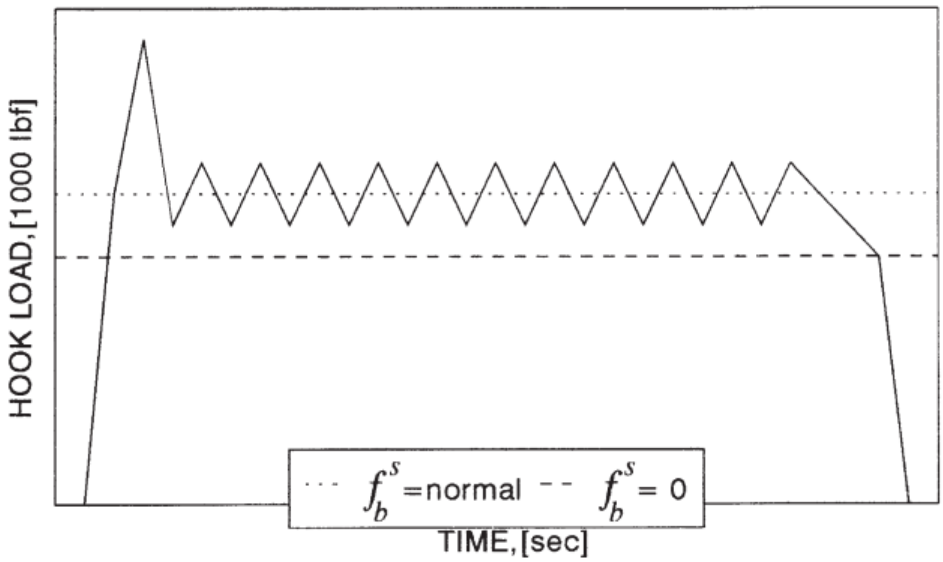

Figure 4: Normal Tripping Conditions in Vertical Well (Cordoso et al., 1995)

Since the experiment of this paper does not include obstructions the initial prediction was that the results would come out somewhat similar to Figure 4.

Field data from a Gullfaks well by Statoil was acquired in order to look at how the HKL acted in the field. A complete drilling operation data in a Matlab type file was acquired for analysis. From the data a tripping operation of the whole drill string was found and is presented in Figure 5. When zooming in the tripping of several stands can be seen in Figure 6. The HKL in the figures is located in the second data column together with the block position (BPOS). 12 stands were tripped consecutively in Figure 6. One of the stands was picked out for a better analysis (see Figure 7). During the tripping of that stand the HKL behaved very linearly, with no oscillating behavior after the initial peak. The static friction factor was approximately the same as the dynamic friction factor, because the HKL during the dynamic state was as high as the initial HKL peak.

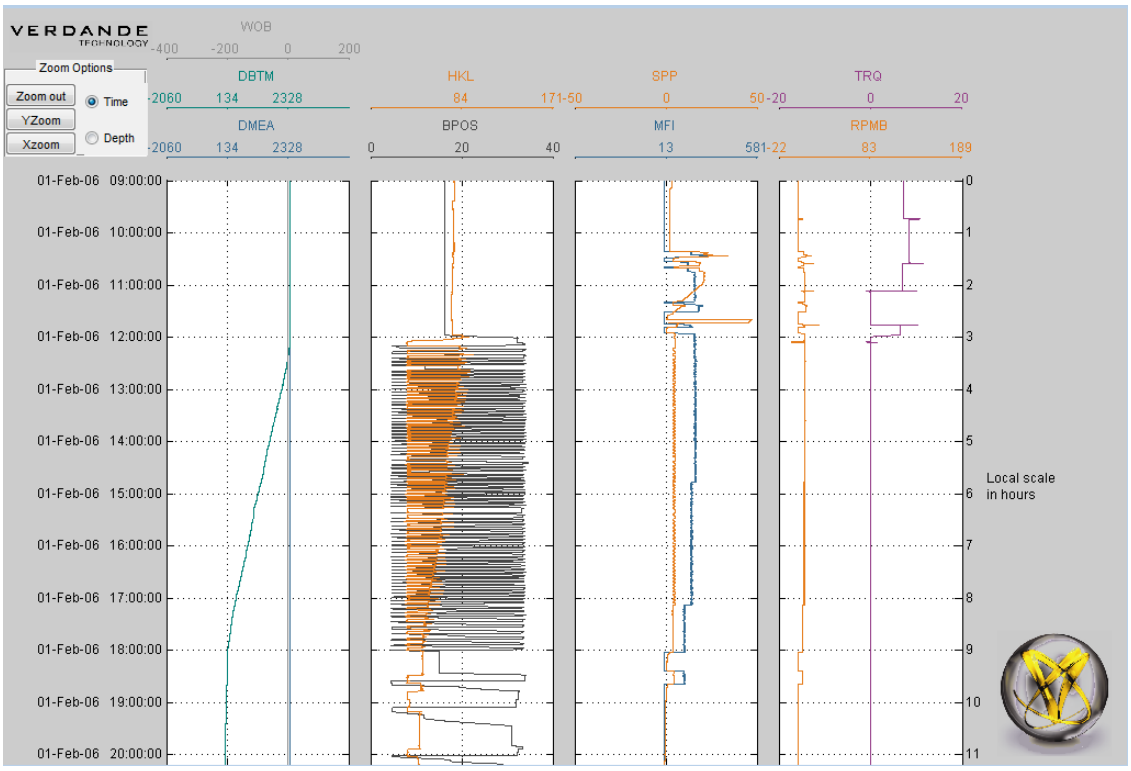

Figure 5: Field Data Whole Drill Pipe Tripping Operation (Statoil, 2007)

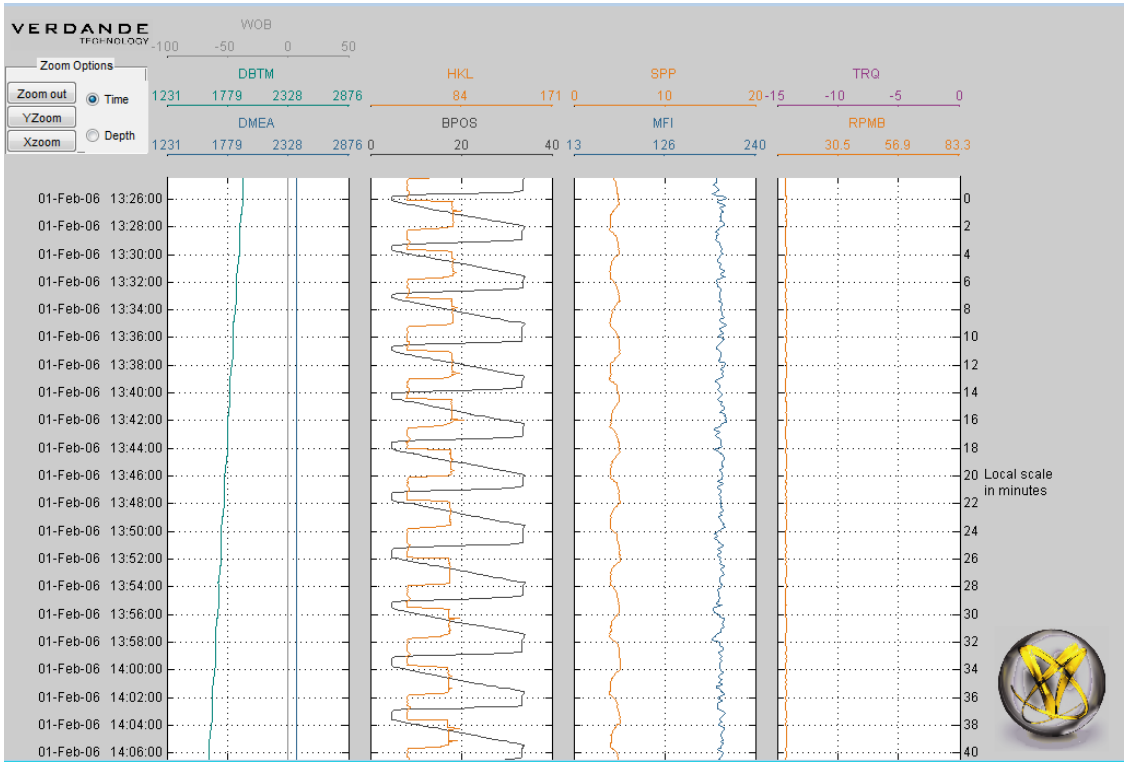

Figure 6: Field Data Several Stands Tripping Operation (Statoil, 2007)

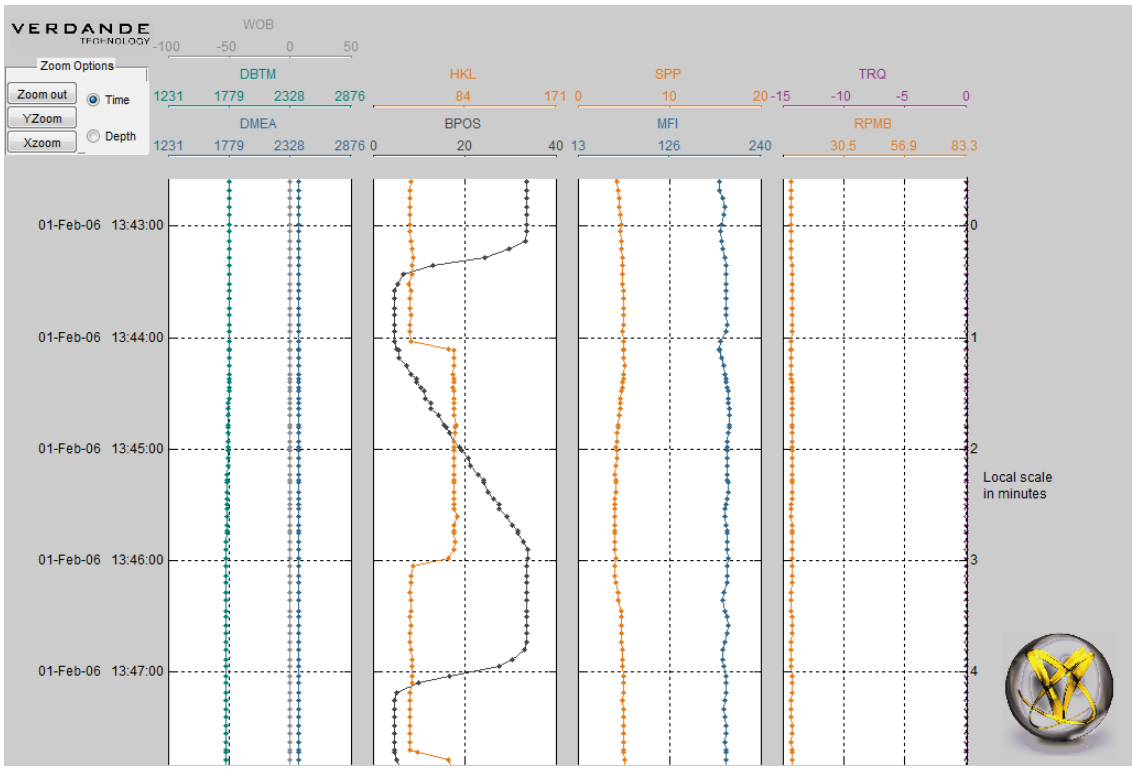

Figure 7: Field Data One Stand Tripping Operations (Statoil, 2007)

3.4. Poor Bore Hole Conditions

There are a lot of uncertainties when it comes to the wellbore conditions, due to the limited data. “Going in blind” is an expression that describes this type of operation. There is no way to see what the bore hole looks like on the inside, and so the main tool for understanding the conditions in the well during tripping is the HKL measurement readings. When the HKL readings differ from the ones seen in Figure 4 the readings are defined as abnormal (Cordoso et al., 1995). There are many causes for these abnormalities, but the most common ones are:

- Cuttings Plowing/ Pack Offs
- Swelling Wellbore
- Creeping Wellbore
- Cavings
- Wash Outs
- Ledges
- Dog Legs
- Key Seats
- Differential Pressure Pipe Sticking

More detailed information on the effects of these specific pore wellbore conditions on the HKL was found in several of the reference materials used for the present work (Cordoso et al., 1995, Sjøbrend, 2014, Bjerke, 2013). For the purpose of staying more on topic, it was not included.

4. Mathematical Model of Peak Behavior

A mathematical model was created to simulate the present work. The more elements included in the model, the more accurately it simulates field tripping operations.

4.1. Supportive Knowledge of the Models

Two models attempted to simulate the HKL during a tripping operation. The non-elastic model was simple and did not require any initial conditions. The elastic model required initial conditions, which were not acquired in the laboratory experiment. The elastic model required initial conditions because the position of the moving drill string changed relative to the position of the moving BHA due to elastic behavior in the drill string and friction forces along the string. Instead the mass-spring model is presented as an example of a model that includes elastic behavior in the drill string (Mme, 2012).

Non-elastic Model

The non-elastic model consists of two HKL equations that express the force; the static state and dynamic state. It assumes a constant, continuous and horizontal surface, like in the experimental rig.

The friction force in static state is expressed as:

$$F_{sf} \leq \mu_s \cdot F_N \tag{13}$$

The friction force in dynamic state is expressed as:

$$F_{df} = \mu_d \cdot F_N \tag{14}$$

The model simulated the increasing HKL as tension in the drill string increased. When the HKL overcame the static friction force, less force was required to keep the BHA in motion, causing the HKL to suddenly drop, and stay constant. This is demonstrated in Figure 3 above.

Elastic Model

The mass-spring model includes more elements than required in the present work. The model takes into account the inclination of the well and the viscous drag force of the drilling fluids, including the buoyancy factor. The present work was done on a horizontal plane with no circulating fluids.

The mass-spring model is built on the following equations (Mme, 2012):

$$m_1 \cdot a_1 = k_{1,2} \cdot \left(x_2 - x_1 - \Delta_{1,2}\right) - F_1 - F_{D1} \tag{15}$$

$$m_2 \cdot a_2 = k_{2,3} \cdot \left(x_3 - x_2 - \Delta_{2,3}\right) - k_{1,2} \cdot \left(x_2 - x_1 - \Delta_{1,2}\right) - F_2 - F_{D2} \tag{16}$$

$$m_n \cdot a_n = HKL - k_{n-1,n} \cdot \left(x_n - x_{n-1} - \Delta_{n-1,n}\right) - F_n - F_{Dn} \tag{17}$$

$$F = \beta \cdot g \cdot m \cdot (cos\alpha + \mu \cdot sin\alpha) \tag{18}$$

$$F_D = \frac{\pi \cdot d_s(dx) \cdot \mu_{viscosity\ mud} \cdot v}{d_h - d_s} \tag{19}$$

The drill sting is modelled as multiple masses linked together with springs as shown in Figure 8.

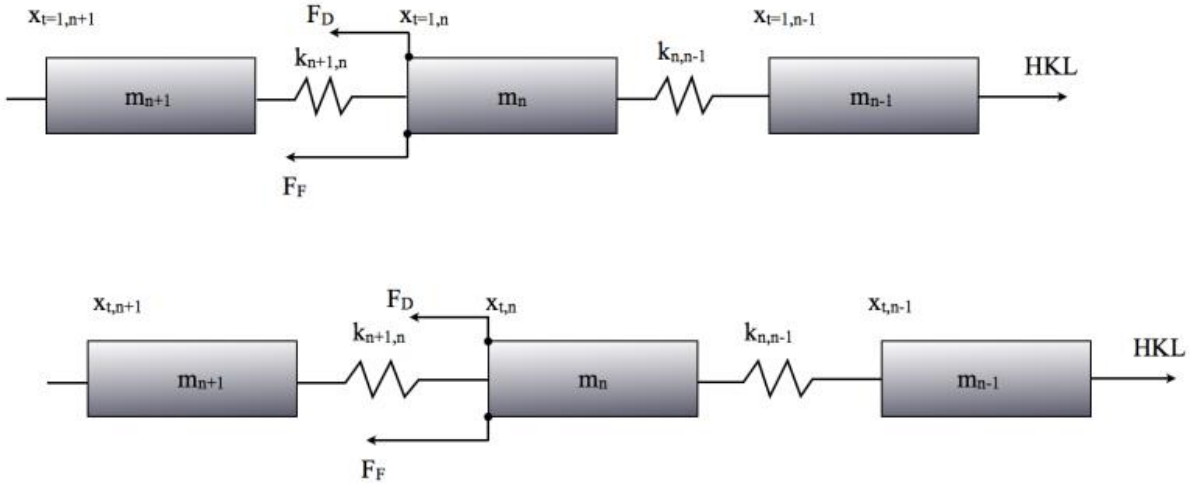

Figure 8: The Mass-Spring System. Above at initial time, below at time step t (Glomstad, 2012)

The HKL is the sum of all the forces acting on every single mass. F_D is the drag force of the circulating drilling fluids, while F is the force of a specific mass including its buoyancy,

friction and weight. The elasticity of a specific spring is expressed as k. The positions of the individual masses are expressed as x, while the initial distance between the masses is expressed as Δ.

4.2. The Model of the Dynamic Peak

A non-elastic model is presented in Figure 9. The tension increased in the static state and then drops as the BHA starts moving. Without elastic behavior the HKL stayed constant once the friction coefficient changed.

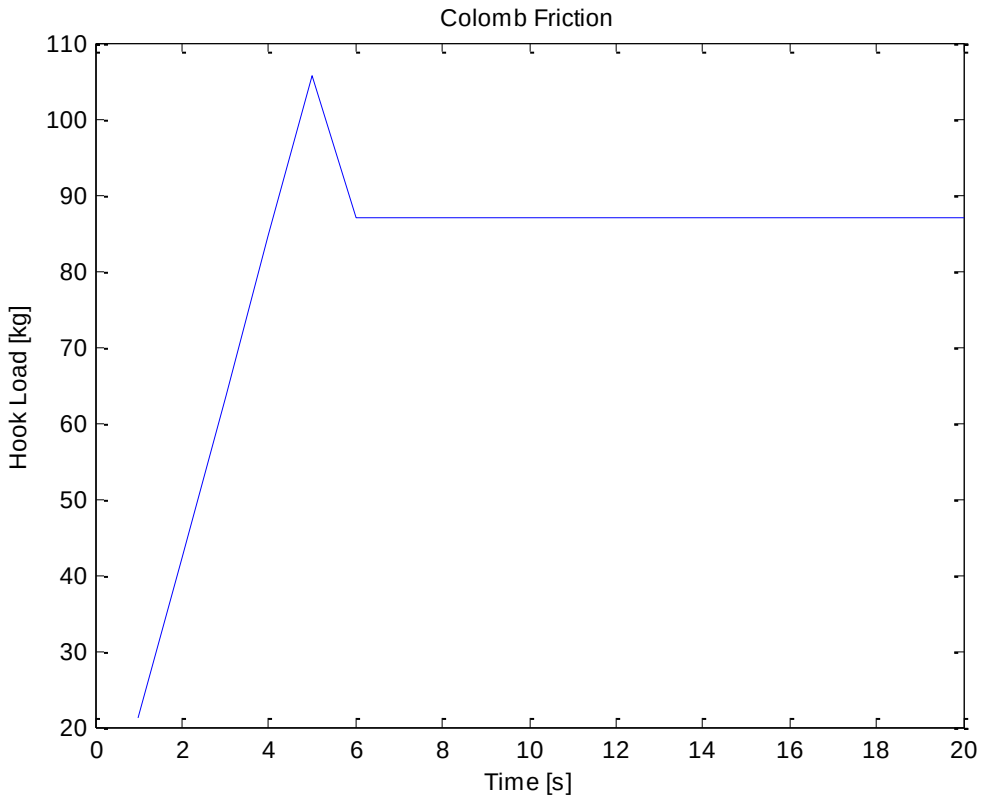

Figure 9: Matlab; Simple HKL Model of Experiment

The program is based on basic friction calculations and with a changing friction factor as the HKL overcomes the static friction.

5. Experimental Investigation of HKL

The purpose of the experiment was to record the initial HKL when simulating tripping operations in a horizontal well in order to compare the results with field data and the model.

Most of the work performed in this project was focused on the experimental investigation. Planning and scheduling was done in order to build the laboratory experiment, to be able to test its functionality and to obtain some initial results. The rig needed to be designed, built and quality checked. Schedules and action plans were made in order to monitor the progress.

The fundamental set up of this experiment was based on previous work, mainly done by Sjøbrend (2014) and Glomstad (2012). The focus of the present experiment was to better understand the very initial hook load during tripping operations in normal conditions, with no physical obstructions involved. It was planned to simulate a tripping operation by pulling a heavy object across specified surfaces by means of wire/winch. To create the elastic behavior of a drill string, springs were integrated in the wire. The HKL and drill string (wire) velocity were the two parameters measured during tripping. The measured signals were sent to a router, which collected the signals into a computer and then processed by a pre-installed software (LabView). The final experimental set up turned out as presented in Figure 10.

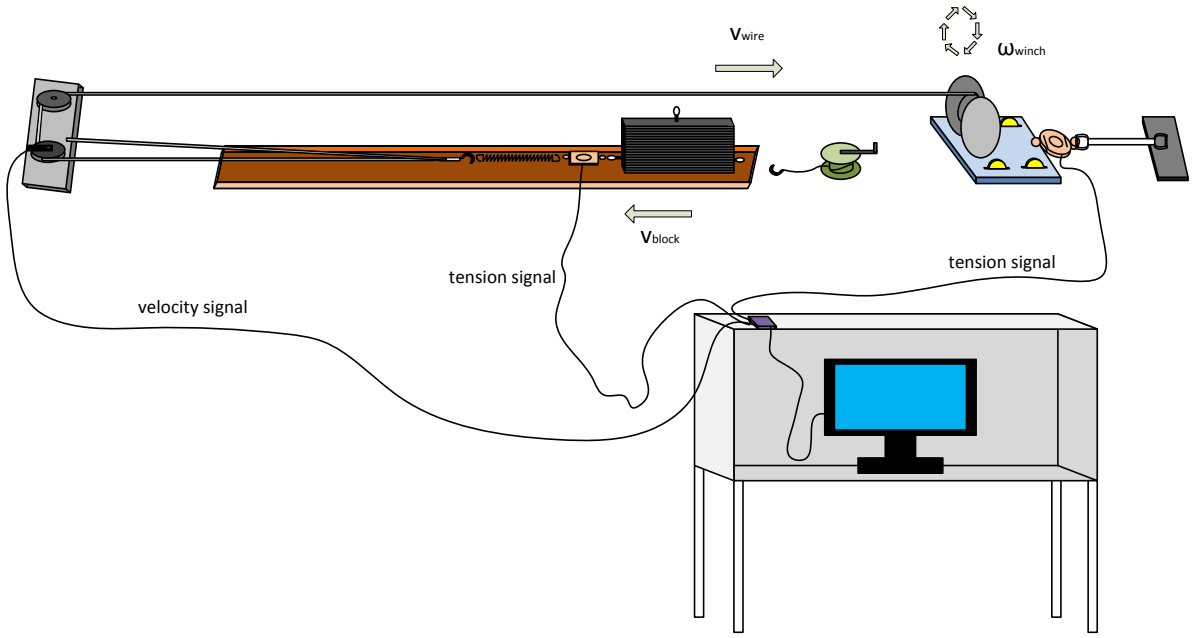

Figure 10: Set Up Design in 3D Perspective

As seen in Figure 10, two tension meters and a velocity meter were wired up to the computer. The HKL rig was custom built and had a sturdy and robust design to endure heavy forces. The rig was also built with hindsight of future work with the set up.

5.1. Design of Lab Experiment

The experiment was given very limited space in the laboratory hall. It was pinned between a wall and a SINTEF experiment, allowing for only 0,93 cm of width for the HKL rig. This made it a bit problematic and difficult for personnel to operate in this narrow space. For future reference and work, it is recommended to have more space. Looking at the work space schematics in Figure 11 the limited space becomes apparent. The length of the HKL rig space measured 13,8 m, which was long enough for the rig, even though it needed to use a loop with a pulley system to shorten the total required length (see Figure 12). The work station space was designated for the computer set up, and for future equipment.

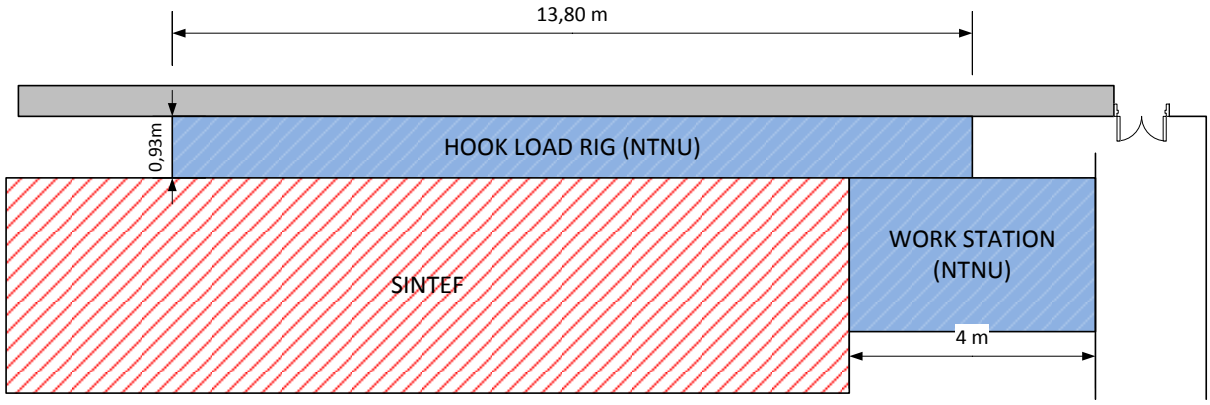

Figure 11: Work Space Schematics

The complete rig is presented in Figure 12, including some equipment that will be used for later experiments by PhD student Isak Swahn and other Master's students. Swahn's set up includes a 9 meter long pipe (annulus) with a fluid circulation system, pumping drilling fluids and cuttings through the pipe while tripping. For present work the focus was on the initial hook load when tripping a metal block (BHA) across different horizontal surfaces without other restrictions.

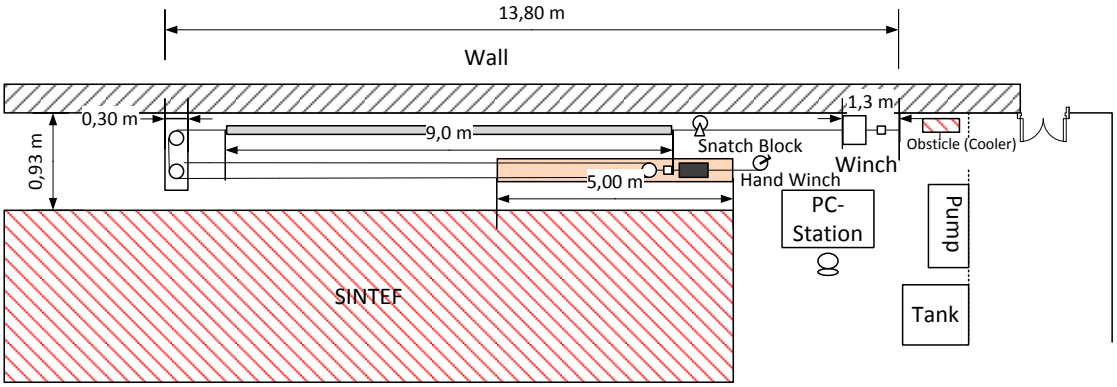

Figure 12: Design Overview of Hook Load Rig

The rig was designed to pull the BHA in a tray using a winch and a pulley system. The wire was reeved through a couple of sheaves and looped back to the winch through a 9 meter long annulus (pipe). In order to measure the tension in the drill string one tension meter was placed behind the winch and another in front of the BHA. When pulling the block the wire velocity was initially planned to be measured in two places, at one of the sheaves at the end of the rig and at the winch. The reason for measuring two velocities was due to the installed springs. The velocity needed to be measured on either side of the springs. A pulley system was put in place for two reasons. Firstly, because of limited space. By making a two-wire-line pulley system the BHA only needed to be pulled half the traveling distance of the wire. This allowed the wire to travel 9 meters without any problem for future runs when an additional BHA will be integrated on the wire in the pipe. The tray containing the different surfaces was designed to let the BHA travel at least half of the pipe length. Secondly, it reduced the pulling force required by the winch. This was mainly for future work when higher forces will be applied with the winch due to the restrictions in the annulus.

Because the process of building the rig took longer time than expected, some components, not necessary for the present project, were left out. The pipe was not installed, and the springs were integrated right in front of the BHA instead of inside the annulus. This made it relevant to measure the wire velocity only over the pulley sheave at the end of the rig. The design in Figure 10 shows how the winch was made with custom designed wheels in order to more accurately measure the tension on the winch's end. Behind the winch a tension meter was attached between the winch and a plate bolted to the concrete floor. The arrows over the

winch indicate the rotation of the winch during tripping, while the other arrows show the direction of the wire and BHA movement. The computer acquired data from three sources; a dynamo placed in one of the sheaves to measure the velocity, a tension meter in front of the block and the tension meter behind the winch. A hand winch was later installed at the end of the tray. Different springs (see Table 3) were placed, one at a time, ahead of the tension meter in front of the BHA.

5.2. The Schedule of Erecting the Rig

The Complete Schedule of lab work from design to testing is presented here:

- Design Test Facility
    - Create initial design in Visio
    - Confirm the physics and reliability of design
- Procurement
    - Create list of items and tools needed for building the design
    - Confirm the list and ordering items
- Build and Pre-test Rig
    - Assemble the procured items as designed
    - Set up the designed rig
    - Confirm the model is made right
    - Set up and learn LabView
    - Pre-test all the parts separately and the whole system together
- Design lab experiments
    - Create the Test Matrix
- Test BHA under different conditions
    - Prepare the HKL rig
    - Run the experiments
- Analysis of lab results vs. field data

Scheduling was a key tool to completing the HKL rig and running the experiments. When the schedule was created it became easier to see the current status. Changes were made along the

way as the design changed due to limited time. The schedule also benefited the lab technicians, as their work was crucial to the project.

Smaller schedules (local action plans) were also created to revitalize motivation and push for milestones, which helped the completion of the project. As time went by it became apparent how things needed to speed up if the rig was to be completed. There were a few setbacks that consumed a lot of time, like when the shipping of some material was delayed, or when the springs, went missing, and new ones had to be ordered.

Table 1 shows the final schedule for completing the rig erection. A lot of the operations were not completed in March, and so the work needed to be sped up the following month. The constant visits to the lab and the lab technicians pushed the completing of the rig, and made it possible to perform some test runs before the end of April.

Table 1: Action Plan During Building of the Rig

	March				April				May			
	11	12	13	14	15	16	17	18	19	20	21	22
Seat for test pipe			●	●	●							
Test pipe w/ connetions		●	●	●	●							
Metal block	●	●	●	●								
Plate for Winch w/ wheels	●	●	●									
Tensiometer to winch and plate on floor		●	●	●								
Tray w/ edges						●	●	●				
Plate for pulleys w/ deadline bolt			●	●	●							
Breaking block		●	●	●								
Velocity meter				●	●	●	●					
Hooks (4)			●	●	●							
Table w/ cabin			●	●	●	●						
Where is cuttings/dolomite	●	●	●									
Springs (Lesjøfors) max 160 daN	●	●	●	●								
Mounting winch-plate	●	●	●									
Mounting sheaves on plate		●	●	●								
Preparing the electronical equipment						●	●	●				
Wiring the the righ to computer								●	●			
Testing the HKL rig								●	●			
Running experiment										●	●	●

Before the experiment was designed the goal of the investigation was defined. A suggested lab design was made shortly thereafter. The design needed to be approved by Pål Skalle, the project supervisor, and by Håkon Myhren, the lead lab technician on the project, before the procurement and building could start. As the materials started arriving the building process commenced.

Once the HKL rig had been assembled, the computer was installed with LabView and wired up to the HKL rig equipment for data processing. LabView acquired and processed the

measurements during tripping operations. Nobody at the petroleum department had much experience with LabView, so a lot of work was put into learning how to use the software and custom creating a processing program that acquired, read, processed and presented the results. The time needed for understanding and using LabView was not accounted for initially, and required more time than expected, delaying the experimental runs over a week.

5.3. Procurement of Material and Equipment

The complete procurement list is presented in Table 2. The items were specified so that when acquired they would have the right dimensions and could be built efficiently. The list specifies the dimensions, type of equipment and material needed. The list also shows the procurement status of the material and instruments at a specific time during the procurement process. The gray items are for future projects.

Table 2: Procurement List. Status as of April 15th

NO	Item - Material		Specifications	Technical Comments	Respon-sible	Status %
1	Pipe		8-9 m, 60 mm OD; 54 mm ID	For later use. Serie coupled, internal flush.	Håkon	
2	Spring		2 t + 1 t + 0.5 t + 0.3 t + 0.25 t	5; strength depending on where spring is mounted	Robin	100
3	Wire		2 t, 40 m; 8mm OD	Wire on wheel is an integrated part of the winch	Håkon	100
4	Pulley		2 t; 160 mm OD	3 single grooved wheels	Robin	80
5	Floor Plate		a) 0.6 m * 0.5 m, b) 0.5 m * 0.3 m	2; bolted to floor. a) for winch, b) for pulley	Håkon	90
6	Tray		Flat steel (0,3 m ·5,0 m), 4 cm steel rims	For creating difeerent friction regimes while pulling the block	Håkon	65
7	Metal block		200 kg - 0.6 * 0.2, with hook	10 * 20 kg metal plates welded together	Håkon	100
8	Tank		150 l, with cuttings separator	For later use	Pål	
9	Trolley for winch		4 wheels	Wheels outside the trolley plate to obtain max vertical stability for	Håkon	90
10	Cabin for PC			SEE 3D DRAWING	Robin	0
11	Sand / Cuttings			1-4 mm limestone particles	Pål	70
NO	Item - Instruments					
1	Winch		2 t	17.5 cm OD drum, 19,9 cm width. Max velocity = 1 m/s	Håkon	100
2	Velocity meter		Mechanical dynamo	2; mounted on winch and on pulley	Åge	100
3	PC, Labview				Lars	70
4	Tension meter		2 000 kg + 200 kg	Amplifier on deadline and winch	Åge	100
5	Pump		Max 1000 lpm	For later use.	Håkon	
6	Pressure transduser		Differential	For later use.	Åge	

The items were procured continuously as the building process commenced. Some of the items like the winch and tension meters were already in possession by the department.

5.3.1. Equipment Specification

Present HKL rig required most of the equipment custom designed. Figure 13 shows a more detailed design of the equipment before the rig was simplified due to limited time.

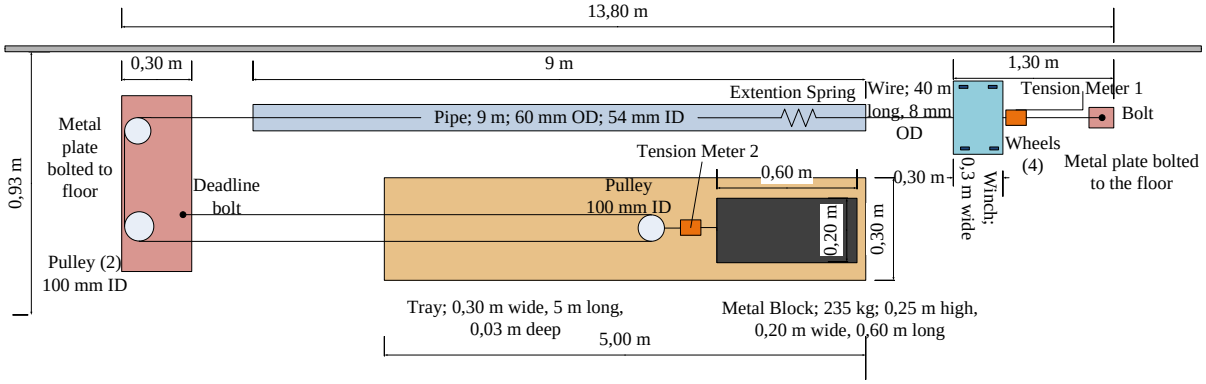

Figure 13: Detailed Equipment Design

Winch

The winch had a 17,5 cm OD drum that reeled in the wire. It was bolted to a new and larger steel plate attached with new custom designed wheels (see Figure 14). This would allow for measuring the tension at the winch-end of the rig. The winch also had an operating box that regulated the frequency of the drum rotation.

Figure 14: Winch and Motor; Simulating the Draw Works on a Drilling Rig

Hand Winch

The hand winch was installed later in the process when it was realized how heavy the BHA was, and how much energy and strength was required in order to pull it back to its initial position after each run. It is also required for future cases of stuck BHA in the test pipe. The hand winch as seen in Figure 10 consisted of a drum and two gears that moved when rotating the handle. A 4 mm wire with a hook attached to the end was reeled in when hooked on to the rear end of the BHA.

Wire

The wire had on outer diameter (OD) of 8 mm, a length of 40 m, and was capable of withstanding 2 tonnes of force. It was not necessary to use such a strong and thick wire for this project, but it was selected so that it could be used in future experiments that will be tripping with much higher force in order to overcome restrictions.

Metal Block

For present experiment the BHA was simulated by a steel block consisting of 10 steel plates welded together. Three rings were attached, in order to move it forward and backward, and for lifting purposes. The block had a mass of 235 kg, being 0,6 m long, 0,2 m wide and 0,25 m high (see Figure 15).

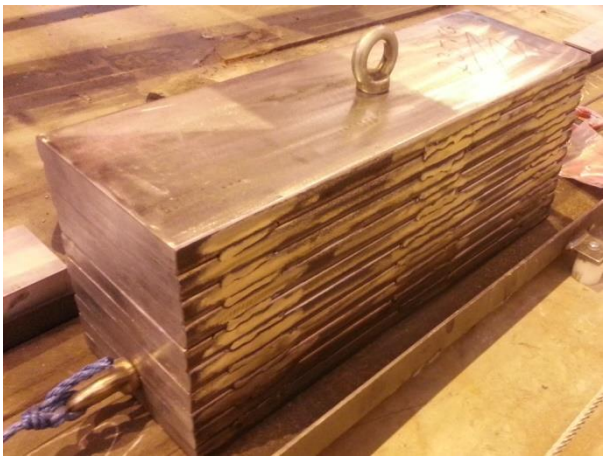

Figure 15: Metal Block Simulating the BHA

Tray

The tray contained the surfaces for the BHA to slide on. After it was welded together it was 5 m long, 0,3 m wide and 0,03 m deep. The welding made the tray almost water tight, though not completely, as water slowly seeped out. The concrete floor was uneven, so the tray was bolted to the floor on top of small pillars adjusting the level.

Springs

Initially the desired springs were supposed to handle 2 tonnes. After careful consideration, it was concluded that the elastic behavior would be minimal. Five weaker extension springs were procured. The four strongest springs were of the same dimensions, but with different number of active coils, while the weakest was smaller as expressed in Table 3.

Table 3: Specs for 5 Different Extension Springs

Spring Strength	D_t	D_y	L_0	n_v	c	F_0	L_1	F_{max}	m_{max}
High	5	30	120	17	23,5	130	148	3608,0	367,8
Medium High	5	30	200	33	12	130	255	3190,0	325,2
Medium	5	30	280	49	7,9	130	361	2981,9	304,0
Medium Low	5	30	350	63	6,2	130	454	2944,8	300,2
Low	4	25	260	58	4,7	80	350	1725,0	175,8

The maximum permitted pulling force and hanging mass are expressed as:

$$F_{max} = L_1 \cdot c + F_0 \tag{20}$$

$$m_{max} = \frac{F_{max}}{g} \tag{21}$$

The springs with the lowest maximum permitted force were the most elastic and the springs with the highest maximum permitted force were the least elastic. The springs are pictured in Figure 16.

Figure 16: Springs for Drill String Elastic Behavior

Cuttings

The cuttings (sand) was placed on the tray surface for simulating the borehole wall and well cuttings. Originally the plan was to use 1-4 mm limestone particles, but somehow they were incidentally disposed of. Another sack of limestone particles was found. The particle size was 0,5-2 mm. When applied in the tray it was spread to a height of approximately 2 mm for every run.

Tension Meters

Two tension meters were used, Tension Meter 1, which was inserted behind the winch and Tension Meter 2, which was inserted right in front of the BHA.

HKL is normally expressed in Newtons, but the tension meters expressed the tension in kilograms.

Tension Meter 1 (TM2000) had a max load of 2000 kg, while Tension Meter 2 (TM200) had a max load of 200 kg. TM2000 was placed behind the winch because it would experience stronger forces in future experiments. TM200 was never in danger of reaching its max load. Both of them gave the same output signal of 2 mV/V. They both had a power supply of 15 V, which meant the maximum voltage output from both of them could be expressed as:

$$V_{\max out} = 2\,\frac{mV}{V} \cdot 15\,V = 30\,mV \tag{22}$$

Dynamo and Pulley Sheaves

At one end of the rig the wire rounded two pulley sheaves with a diameter of 100 mm ID. They were attached 0,23 m apart to a steel plate that was bolted to the floor. As shown in Figure 17, one of the sheaves had a dynamo installed, rotating together with the sheave. The dynamo was wired up to the computer, which read the voltage produced from the rotation, translating it to linear velocity.

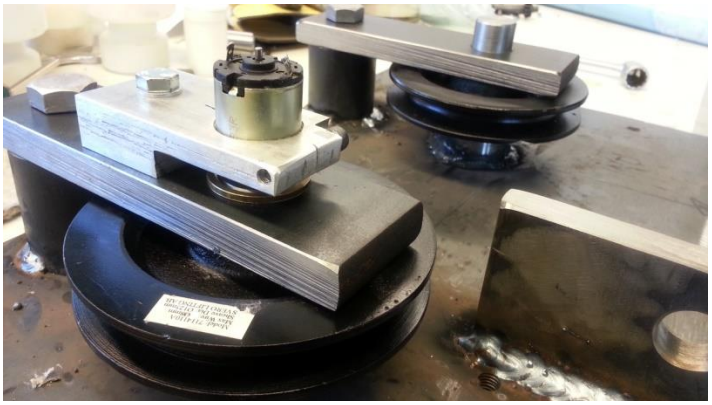

Figure 17: Sheaves with Dynamo

Dynamo Calibration

The dynamo needed first to be calibrated to be able to convert the output voltage to wire velocity. The experimental runs were divided into five velocities. Each of the velocities coincided with a specific winch operating frequency. The relationship is shown in Table 4.

Table 4: Calibrated Wire Velocity

Wire Velocity	Velocity	Winch Frequency
	[cm/s]	[Hz]
Low	2,6	5
Medium	5,1	10
High	10,2	20
Super High	15,3	30
Ultra High	19,4	38
Volt estimate V = 0,245 V		

The wire velocity was calculated from Eq. (23).

$$v = \frac{V_{output} \cdot v_{est}}{V_{est}} \tag{23}$$

Here v is the calculated velocity, V_{output} is the voltage going into LabView, v_{est} is the estimated velocity and V_{est} is the estimated voltage. The velocity and voltage output were linearly related when using this dynamo, and in order to convert the voltage output to velocity it was necessary to calibrate it. This was done by running the winch at three different frequencies, measuring the rotation time for the pulley sheave, and reading the voltage over the same time. The three runs were consistent and linear, so from that, base estimations of the velocity and voltage were made.

The estimated velocity was calculated by dividing the circumference of the sheave by its rotation time, as in Eq. (24).

$$v_{est} = \frac{C_{sheave}}{t} = \frac{\pi \cdot d_{sheave}}{t} \tag{24}$$

The estimated velocity was linear and parallel to the winch frequency and the estimated voltage output. Table 5 shows the voltage output for each of the three estimated velocities. The three voltage outputs consequently became the voltage estimates.

Table 5: Voltage and Velocity Calibration

Voltage output	Time	Velocity
[V]	[s]	[cm/s]
0,48529	3	10,2
0,24548	6	5,1
0,12416	12	2,6

The velocity was not estimated for the increasing diameter of the winch drum. As the wire reeled in and made a new layer of wires the velocity slightly increased.

PC and Cabin

The cabin was designed to shelter the PC in the dusty laboratory environment. The PC needed the Labview software installed in order to create a platform to process the voltages from the different sources. The PC received the information via a USB device, NI USB 6009, which gathered all the analog signals. The PC and cabin set up was shown previously in Figure 10.

5.3.2. Electronics

The most central components of the electronics are displayed in Figure 18.

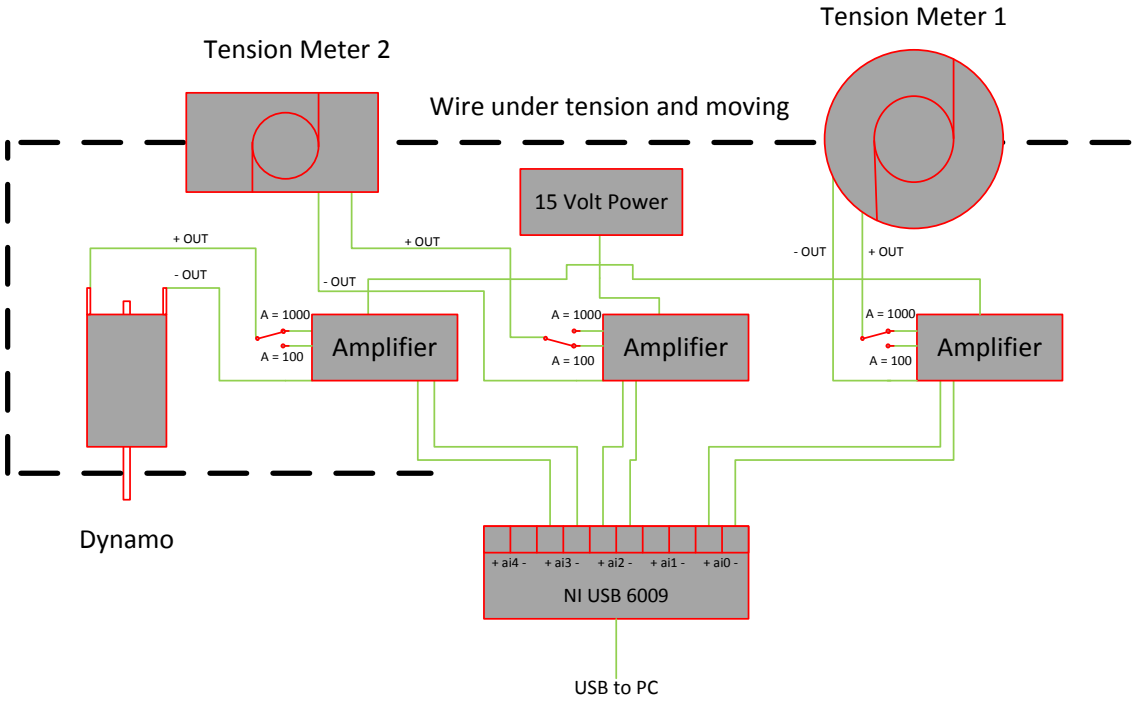

Figure 18: Electronic Schematics for Hook Load Rig (Designed by this author in Microsoft Visio)

All the signal sources received a 15 volt power through three separate power converters (displayed as one in the schematics). The amplifiers could alter the amplification between 100 or 1000. TM2000 and Dynamo signals were amplified by 1000, while TM200 was amplified by 100. The reason for amplifying TM200 by only 100, and not 1000, was to fit all the raw data in the voltage chart in LabView. The data logger gathered and routed the signals to the computer through a USB port.

The signals were disturbed by some “noise”, which created abnormal spikes in the results. This was also reported by Sjøbrend (2014).

5.3.3. LabView

LabView offered a platform to custom design a program for reading and processing the input signals.

LabView used a VI (virtual instrument) platform that allowed the user to create his/her own custom designed processing program. The software had built-in functions for data acquisition that was directed through a self-designed path. LabView had two operating interfaces, the Front Panel and the Block Diagram. The Front Panel displayed the results of the selected VIs from the program (see Figure 19). The program was designed in the Block Diagram where the signals were acquired, read and processed (see Figure 20).

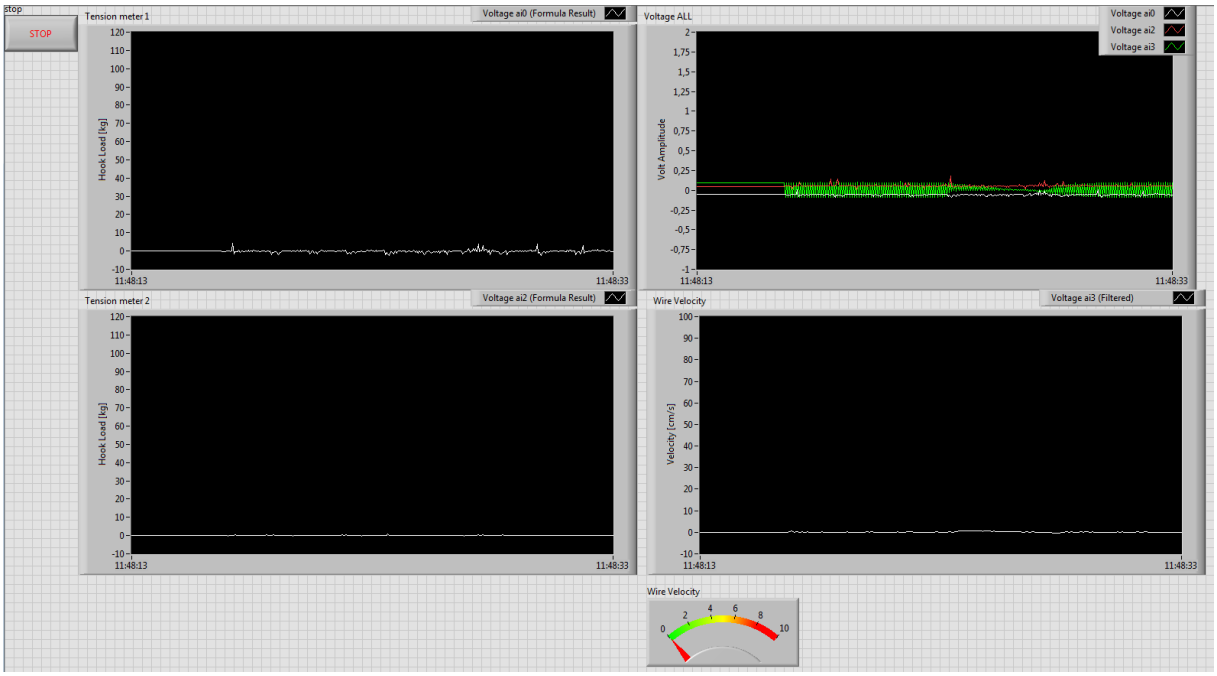

Figure 19: LabView Front Panel shows the following 6 items: Stop button (upper left button), TM2000 (upper left chart), TM200 (lower left chart), Wire Velocity (lower right chart and bottom meter) and Voltage ALL (upper right chart).

The Front Panel consisted of a stop button, four waveform charts and a meter. The tension meter measurements were plotted in two HKL-Time charts. The wire velocity was displayed in the velocity meter for real time measurements, and plotted in a Velocity-Time chart. The last chart showed the raw voltage feed from the three sources in regards to time. The stop button stopped the running of the program manually.

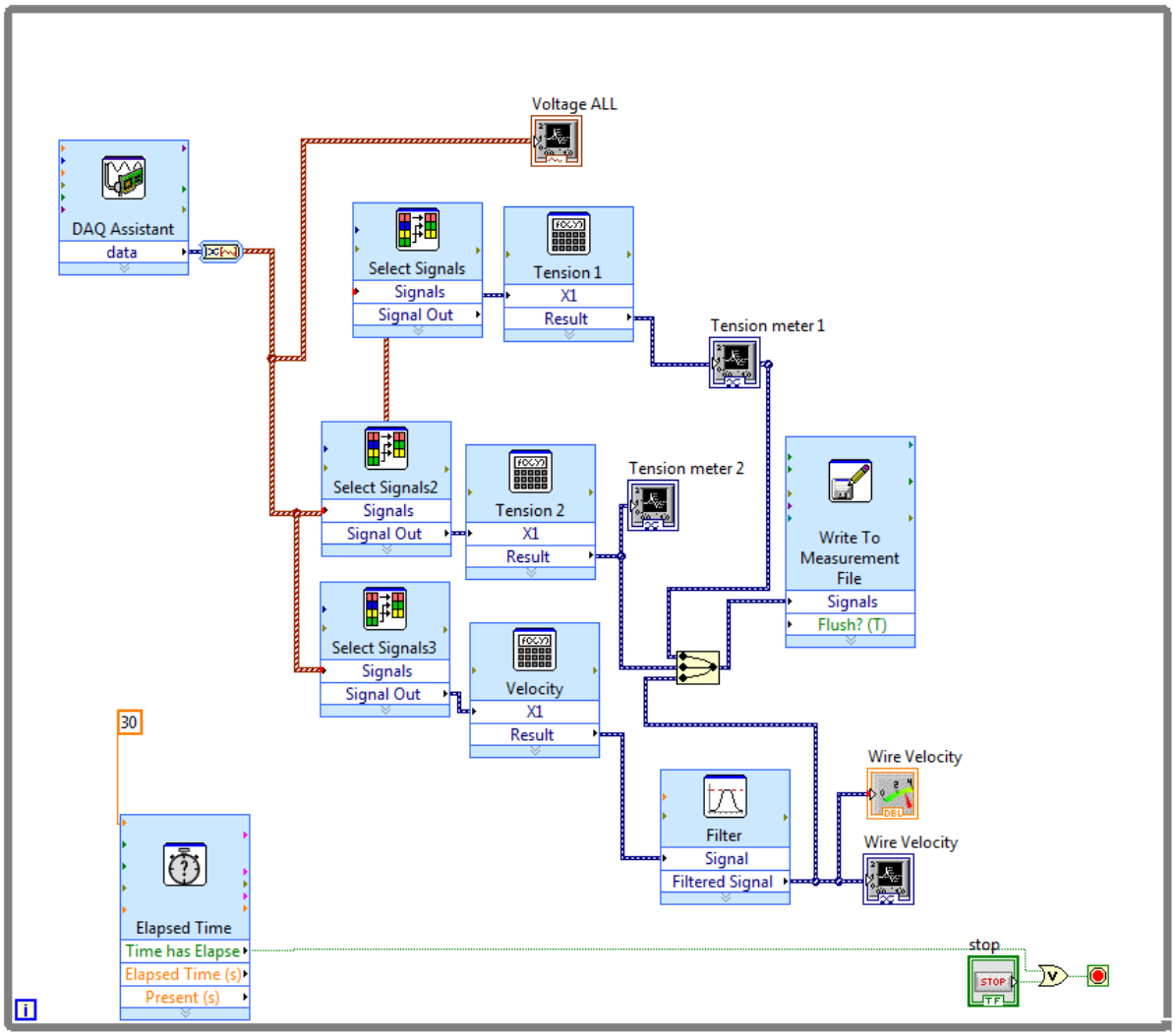

Figure 20: LabView Block Diagram; the signal flow (designed in LabView by this author)

The Block Diagram seen in Figure 20 was the first fully developed program, by which the first 15 experimental runs were performed. It was later modified to remove more of the "noise". The improved Block Diagram is presented in Figure 23.

The DAQ Assistant retrieved the input signals, 1 sample for every 20 Hz, and sent them as a dynamic data to a converter; converting them to a 1D array of waveform. The array went into a waveform chart called Voltage ALL, plotting the raw signal. The signals were also converted into HKL (kg) and velocity (cm/s). Once converted, the signals entered into waveform charts. The velocity signal was given a filter due to its high frequency. The filter was a low-pass filter type with a cutoff frequency at 5 Hz. The three signals were then merged

and written into an excel file including the time laps. A “while loop” enclosed all the components, which ran until the time elapsed or was manually stopped.

HKL translation of TM2000:

$$HKL = X1 \cdot \frac{2000\ kg}{30\ V} + 3{,}641\ V \tag{25}$$

The voltage is $X1$, while 2000 kg is the maximum permitted load of the tension meter, and 30 V (Amplification = 1000) the maximum voltage output. The calibrating constant of TM2000 was 3,641 V.

HKL translation of TM200:

$$HKL = X1 \cdot \frac{200\ kg}{3\ V} - 0{,}347\ V \tag{26}$$

The maximum permitted load for TM200 was 200 kg, and the maximum voltage output was 3 V (Amplification = 100). The calibrating constant of TM200 was -0,347 V.

The velocity translation:

$$v = X1 \cdot \frac{5{,}1\ cm/s}{0{,}2501\ V} \tag{27}$$

Here $X1$ represents all the input signals.

5.4. Test Matrix

An initial test matrix was designed for the experiment, giving an overview of planned runs. The test matrix included the different surface types, velocities, springs (for elastic drill string behavior) and accelerations. All of the variables affect the initial hook load. The idea was to see how the results would compare to normal field friction curves and modeled curves.

The initial activities in the test matrix are shown in Table 6. The number of tests added up to 48 total potential runs. The initial plan was for surface A, the steel to steel friction, to be used as a base line for the rest of the experiment. The run (performed tripping operation) was also

initially going to be executed with only one type of spring, two sets of velocities and one set of acceleration, which reduced the number of runs to 38.

Table 6: Activity in the Test Matrix for Qualifying the Experimental Rig

Activity	**Variation**	**#**
Pulling	slow, fast	2
Pulling acceleration	low, high	2
Spring strength	low, medium, high	3
Block resting conditions	A, B, C, D	4
Comments to total # of tests:		
Total # of tests possible 2·2·3·4 = 48		
Total # of tests desired 2·2·3·3+2 = 38		
Comments to block resting conditions:		
A. Completely dry tray; steel against steel		
B. Water is allowed to enter the contact area		
C. Very viscous mud; sticky filter cake		
D. Sand		

Table 7 shows the test matrix. The surfaces A, B, C and D had different combinations simulating surface conditions inside a well. The three conditions were; dry sand, water-wet sand and mud-wet sand. The different springs simulated different elastic behavior.

Table 7: Initial Test Matrix, with maximum 48 # of runs

Block resting condition	Spring strength	Low Acceleration		High Acceleration	
		Velocity		Velocity	
		Slow	Fast	Slow	Fast
A	Low				
	Medium				
	High				
A+D	Low				
	Medium				
	High				
A+D+B	Low				
	Medium				
	High				
A+D+C	Low				
	Medium				
	High				

Due to time limitations the test matrix was changed in order to complete the project. The mud-wet cuttings was completely excluded together with the acceleration. The reason for excluding the acceleration measurements was due to the difficulty performing the measurements. In the final test matrix two extra velocities were included with the medium low spring strength; super high and ultra high velocity as shown in Table 8.

Table 8: Final Test Matrix, with maximum 45 # of runs

Block resting condition	Spring strength	Velocity				
		Low	Medium	High	Super High	Ultra High
A	Low					
	Medium Low					
	Medium					
	Medium High					
	High					
A+D	Medium Low					
	High					
A+D+B	Medium Low					
	High					

The final test matrix used five different spring strengths for the metal-to-metal surface, while only two for the dry and water-wet sand surfaces. It was concluded that this would be sufficient number of runs in order to get enough experimental data. 25 runs were performed with the new test matrix.

5.4.1. Trial Runs and Quality Checking

There were three parts of the system that needed to work before the actual experimental runs could commence:

1. The Mechanics
2. The Electronics
3. The LabView Program

The mechanics were tested first, before connecting electronic instruments. An operating system controlled the winch with a running frequency. The wire was integrated in the winch, reeved through the pulley sheaves and hooked up to the BHA. The winch ran the wire in both directions. When the wire was unspooled the BHA was reeled back with the hand winch to its starting position. The winch was tested at different frequencies (low and high velocities). The

highest velocity the winch could obtain without shutting down was 38 Hz; the Ultra High velocity.

The signals from the electronic instruments were tested second, after connecting them to the HKL rig. The USB router was first tested with batteries, to see if it could register voltage signals. Voltage signals appeared in the NI 6009 signal reading program on the computer. The tension meters and dynamo were then connected to the router. When tension was put on the wire and the sheaves started turning signals showed up on the computer in LabView.

The custom designed LabView program was tested last, when the other parts of the rig had been approved. This was done through a trial and error approach along with program development. When completed the first program was able to read, process, write and display the results of the signals. The signals were also calibrated in the program. A problem that proceeded to continue throughout the experiment was the continuous disturbances in the signals, referred to as "noise".

"Noise"

The cause of the noise was unknown at first. The noise turned out to be coming from the winch operating system. When the operating system was turned off the disturbances disappeared. Sjøbrend (2014) had the same problem when he worked with the same winch operating system. He worked hard to get rid of the noise by contacted different experts about the problem, and ended up having to use several filters with low cut of frequency in his LabView program.

Before any measures were taken to dampen the noise, the charts looked as presented in Figure 21. Each individual signal was affected to a different degree. The noise made it difficult to get readable results. Different methods were attempted in order to get rid of the noise.

It was believed that the noise, coming from the winch operating system, was due to poor filters. The first attempt was to get the PC and wires as far away from the operating box as possible. Because of limited space and wire length it made little difference.

It turned out that the more the instrument wires were looped into tight coils the more of the noise disappeared in the signals. This was not an ideal method, because the wire length was needed, in order to reach various parts of the rig. Each of the main wires was coiled up as much as possible. With the wires coiled up the new wave diagrams changed as in Figure 22.

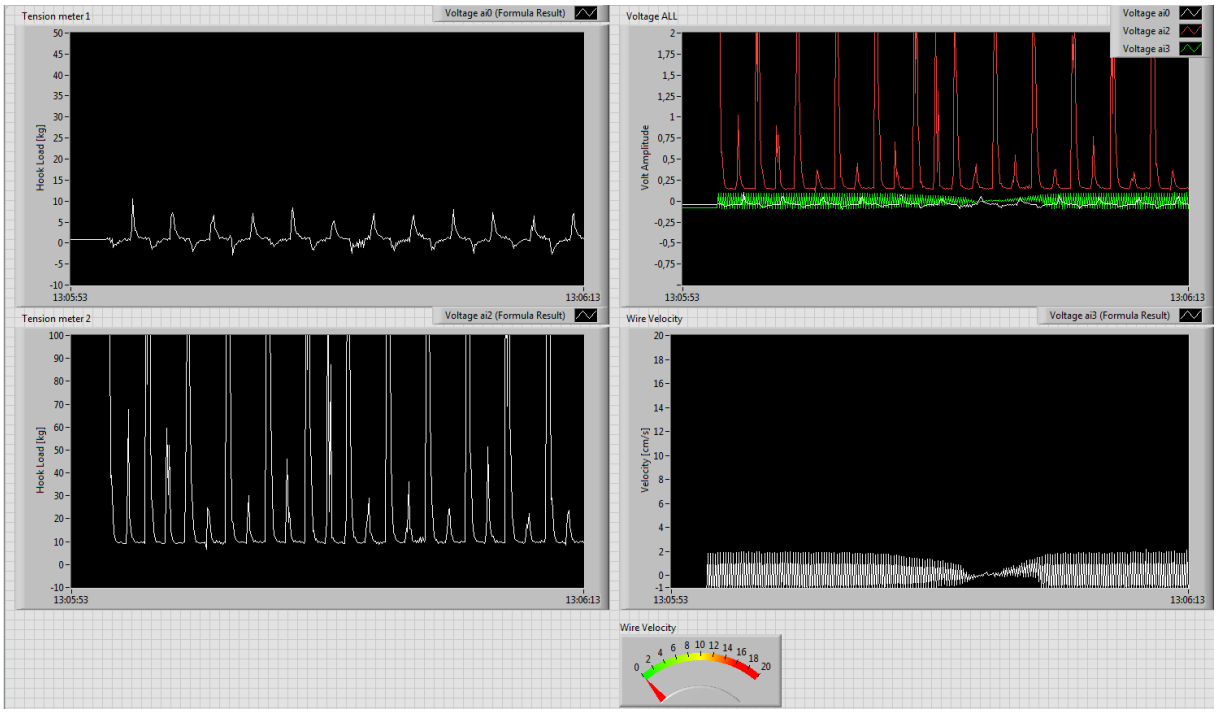

Figure 21: Disturbed Signals

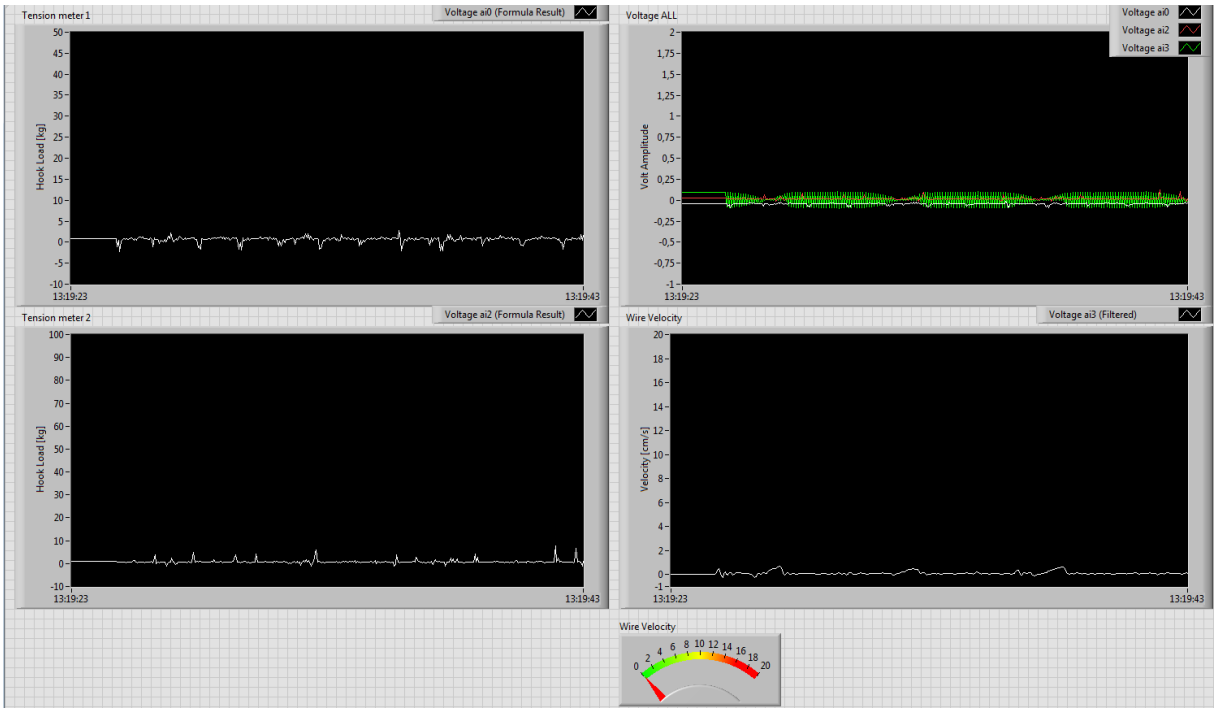

Figure 22: Disturbed Signals with Coiled Wires

The signals became drastically better, even though the noise was not eliminated. The first 15 experimental runs were performed using the coiled-wires set up. The noise was amplified when tension was put on the wire and the sheave rotated.

Even though the DAQ Assistant filtered a lot of the signals by using a lower sampling rate, it could not filter away the noise. Consequently a better filtering system was required in the LabView program. The new custom designed program improved the results and eliminated the noise almost completely. The new Block Diagram included a couple of more filters for the tension meter signals (see Figure 23).

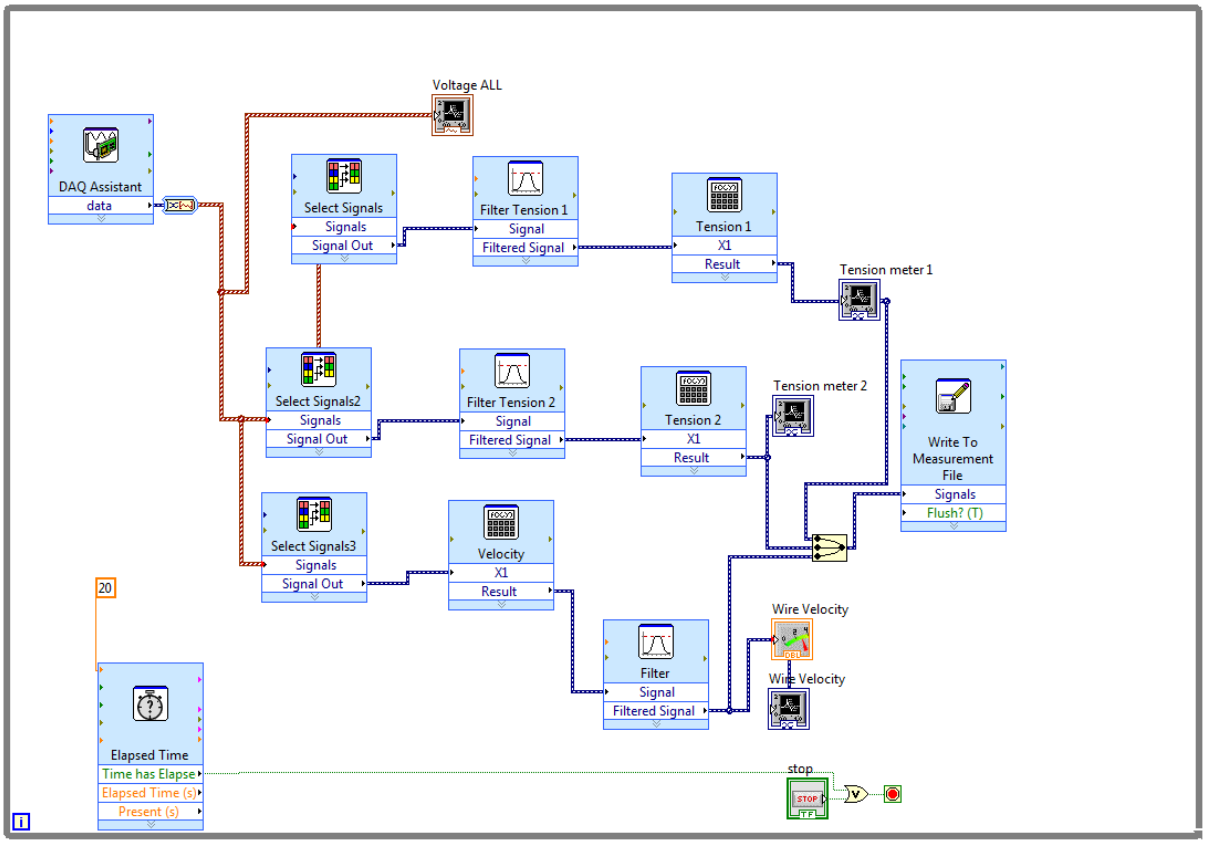

Figure 23: Final Block Diagram; Same signal flow but with higher sampling rate and new filters (designed in LabView by this author)

When the new filters were placed in the Block Diagram the sampling rate of the DAQ Assistant was set to 500 for every 1000 Hz. The new filters were installed with a low-pass filter with a 1 Hz cutoff frequency. The new signals, as seen in the Front Panel in Figure 24, were improved. No changes were made in regards to the wires; they were still coiled up as much as possible.

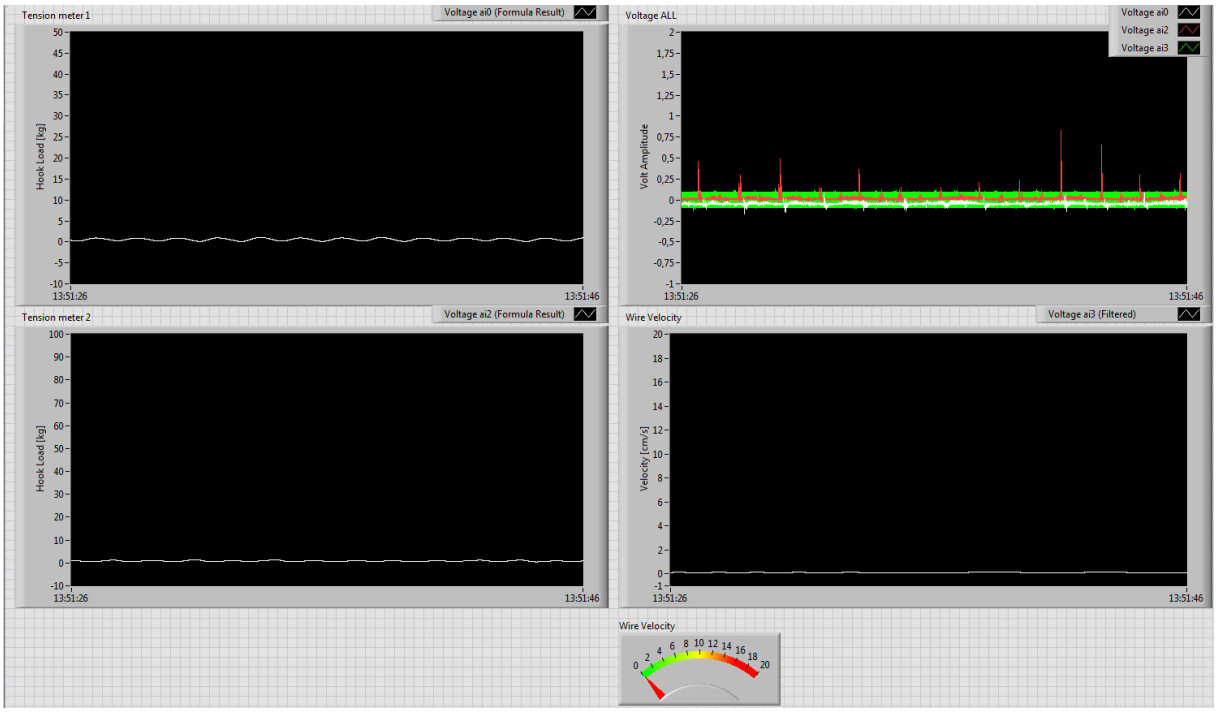

Figure 24: Front Panel with New Filters

The wave chart diagram for TM2000 showed the most signs of noise. Compared to the old noise, this was a major improvement. The Voltage ALL wave chart, shows the increased sampling rate for all signals.

Running Procedure

In order to obtain the most consistent results the procedures were performed and repeated as shown in Figure 25. The new experimental runs were performed according to the final test matrix.

Sand and water required more work, as the BHA needed to be lifted up with a crane after each run in order to replace and refill the sand and water.

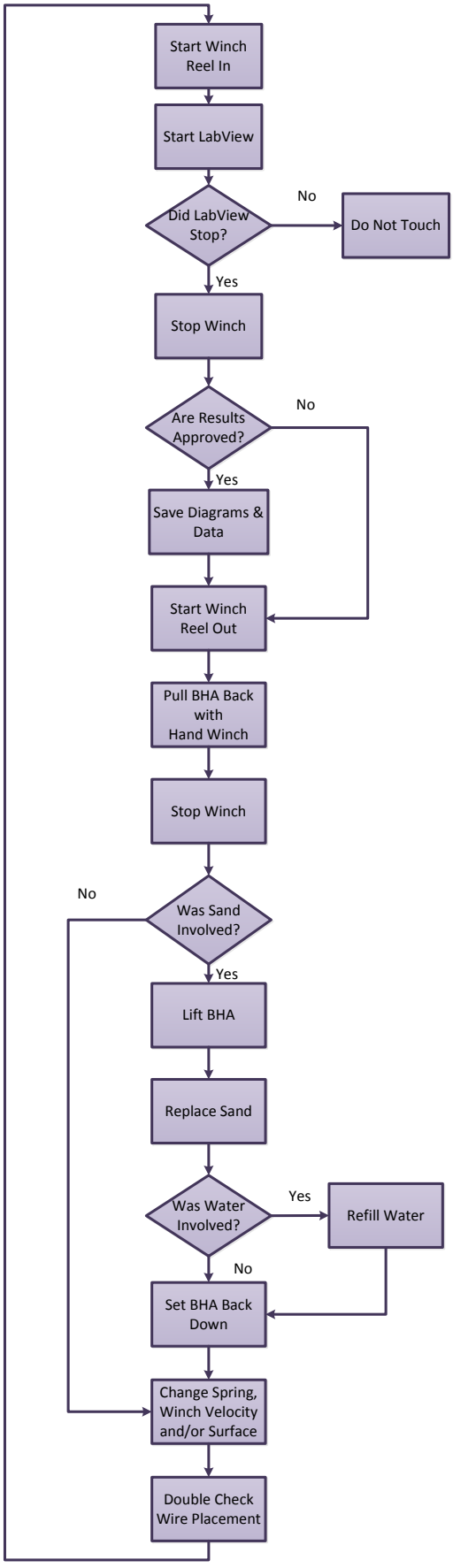

Figure 25: Flow Chart of Running Procedure

6. Experimental Results

The experimental results are shown as LabView outputs. In this section the results are presented, evaluated and analysed. All the results ran over a 20 second time span.

Out of all the experimental results, the most interesting and relevant data was chosen in order to understand how the HKL acts under different conditions. Both the tension meters gave valid results, but because TM200 showed less noise, its data was used for most of the evaluation. Both tension meters showed approximately the same data, but TM200 was more sensitive to the forces restricting the BHA.

6.1.1. Familiarizing with the Results

To better understand the results an introduction to the type of results is presented.

TM2000 vs. TM200

TM2000 showed a tension force of about half of the tension force of TM200 due to the two-wire pulley system (see Figure 26). The scale in TM2000 went up to 50 kg, and up to 100 kg in TM200.

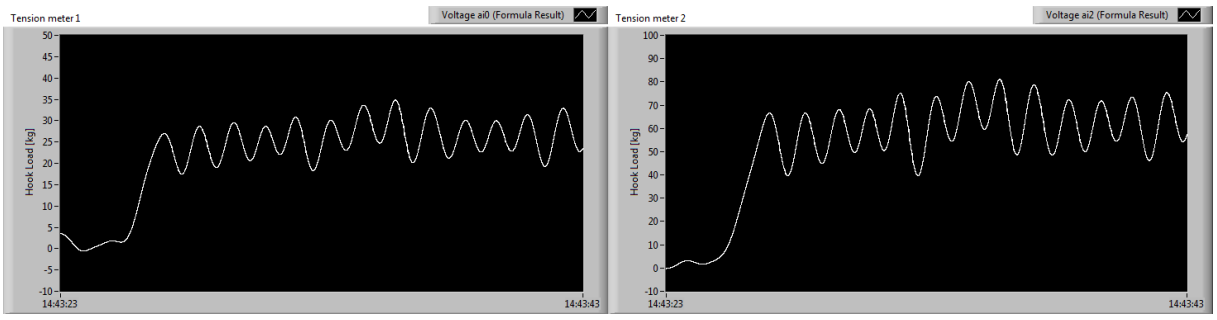

Figure 26: HKL in TM2000 (left chart) and in TM200 (right chart)

The initial HKL peak in TM200 was almost 70 kg, while in TM2000 it was almost 30 kg. Theoretically it should have halved. However TM2000 was affected by the friction forces in the pulley sheaves and under the winch. TM2000 was placed behind the winch, and the winch had wheels to create as little friction as possible. The friction under the wheels still took some of the load off of TM2000. The friction forces under the winch were much greater than in the pulley system, because the friction in the pulley system would have increased the tension, but the results show that the tension was less than half of TM200.

Velocity Signals

The velocity signal showed the wire velocity as the BHA was pulled. The velocity was measure to see if the tension was affected by it, and if the velocity was constant in the system. Four different velocities are presented in Figure 27. The scale for all the velocity charts go up to 20 cm/s, except for the lower right chart, with ultra high velocity, scaled up to 30 cm/s.

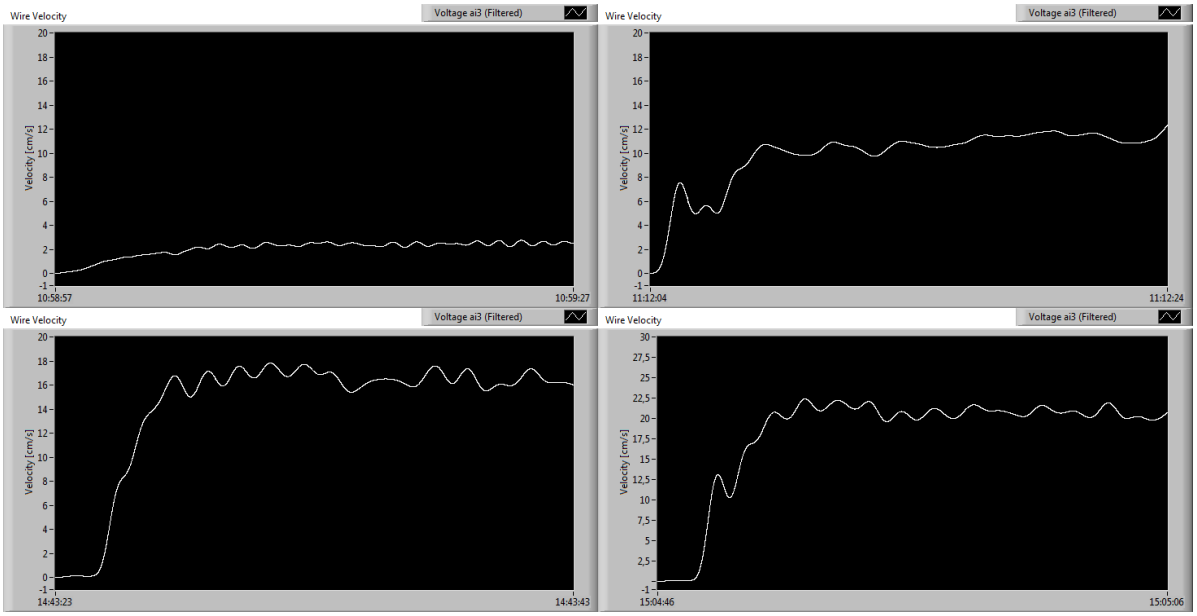

Figure 27: Velocities; Low (upper left), High (upper right), Super High (lower left) and Ultra High (lower right)

The velocity measurements were fairly accurate when compared with calculated velocities in Table 4. The lowest velocity had the more accurate reading because less oscillation in the drill string was involved. Not all the runs had major discrepancies in the velocity as the two charts on the right. This was due to the wire placement in the winch during the spooling. When the wire wound up on itself and then slipped down to a lower level the wire decelerated for a split second.

Raw Data Signals

Figure 28 shows the difference in the sampling rate, between the filtered and the unfiltered program. The left charts show a low velocity while the right charts show a higher velocity.

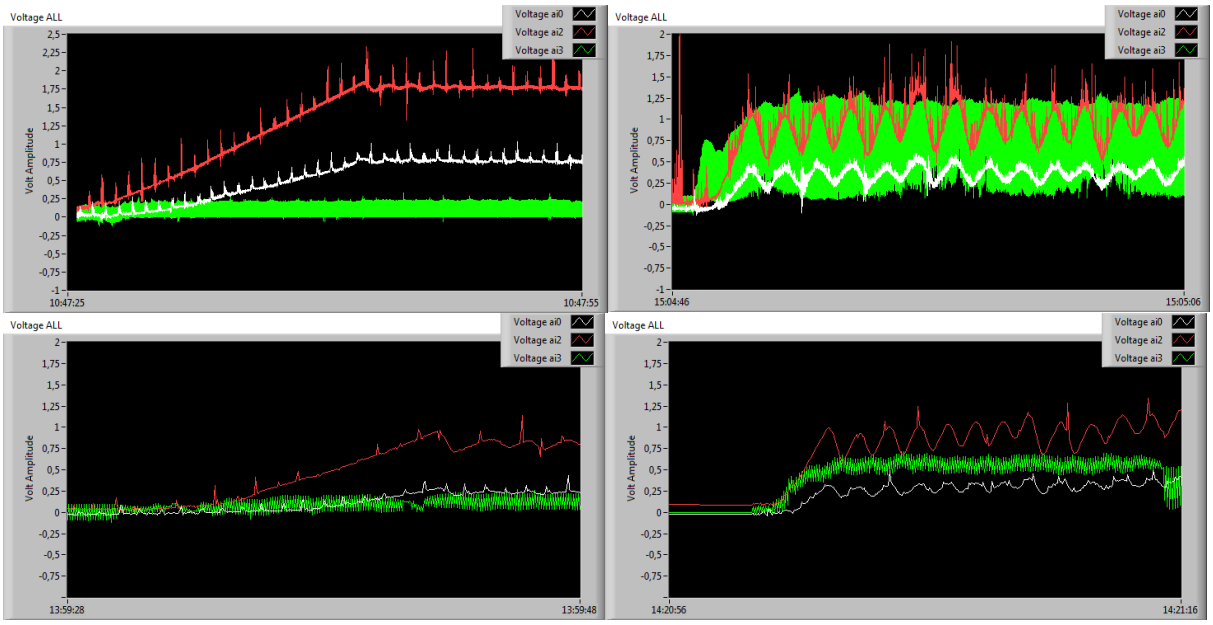

Figure 28: Raw data charts with high sampling rate program (upper left and right) and low sampling program (lower left and right) of low (left charts) and high velocity (right charts).

Plotting the raw data made it possible to observe the input signals before they were converted and filtered. This was done to verify the quality of the signals coming in. The raw voltage data picked up all the noise in the signal. As the sampling rate increased more noise was picked up as shown in the two upper charts.

"Noise" Effect on HKL With and Without Filters

The difference in the HKL measurements before and after the program in LabView was improved is presented in Figure 29.

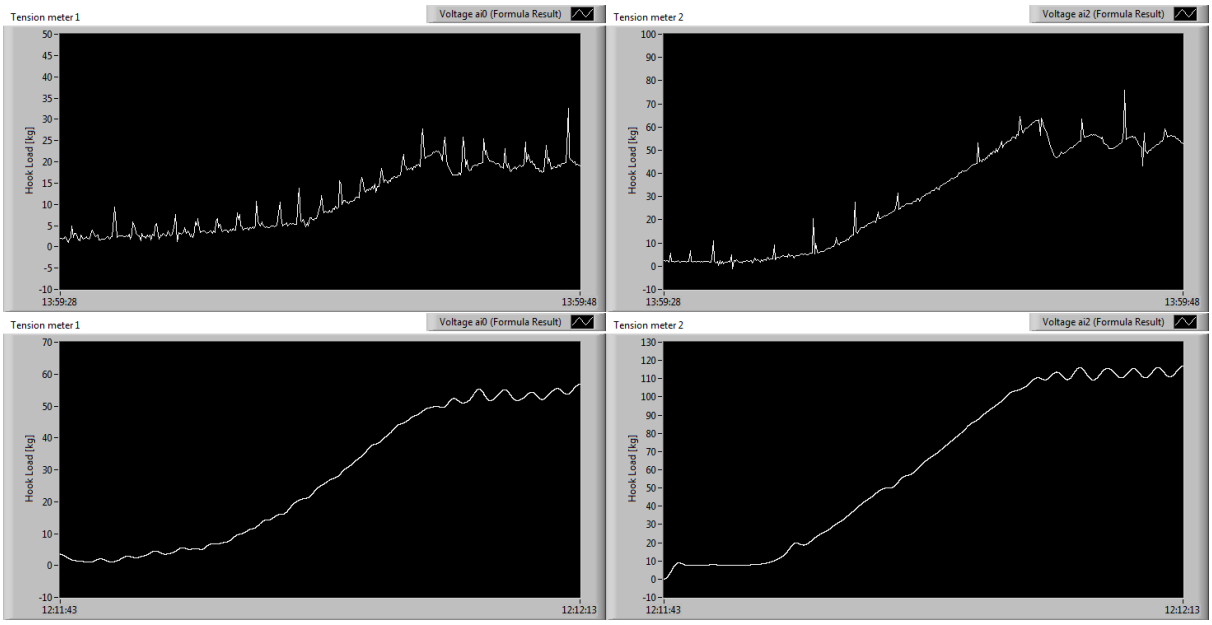

Figure 29: HKL of TM2000 and TM200 from first program without filters (upper left and right) and second program with filters (lower left and right).

The filtered signal curve was not affected much by the noise because the number of samples from the actual signal was so much greater than from the noise.

6.1.2. Result Evaluation

In this section the results are evaluated and compared with some field data and the model. All the results presented in the evaluation were taken from TM200, on order to limit the results in the report. Both the tension meters showed similar curves, but TM200 experienced less interfering friction in the system.

The result evaluation topics are:

a) Metal Surface at Different Velocities
b) Metal Surface with Different Spring Strengths
c) Dry Sand Surface with Two Spring Strengths and Two Velocities
d) Water-Wet Sand Surface with Two Spring Strengths and Two Velocities
e) Three Surfaces with Two Spring Strengths and Low Velocity
f) Three Surfaces with Two Spring Strengths and High Velocity
g) Velocity and Spring Strength Influence on Initial HKL
h) Comparing Experimental Results with Field Data and Model

a) Metal Surface at Different Velocities

The HKL measurements changed as the runs were performed with different velocities. Five different velocities were performed on the metal surface. Super high and ultra high velocities were performed to see if major changes in the velocity would affect the HKL in any new ways. Figure 30 shows all five velocities (low, medium, super high and ultra high) with the medium low spring strength. To see the different velocities see Table 4.

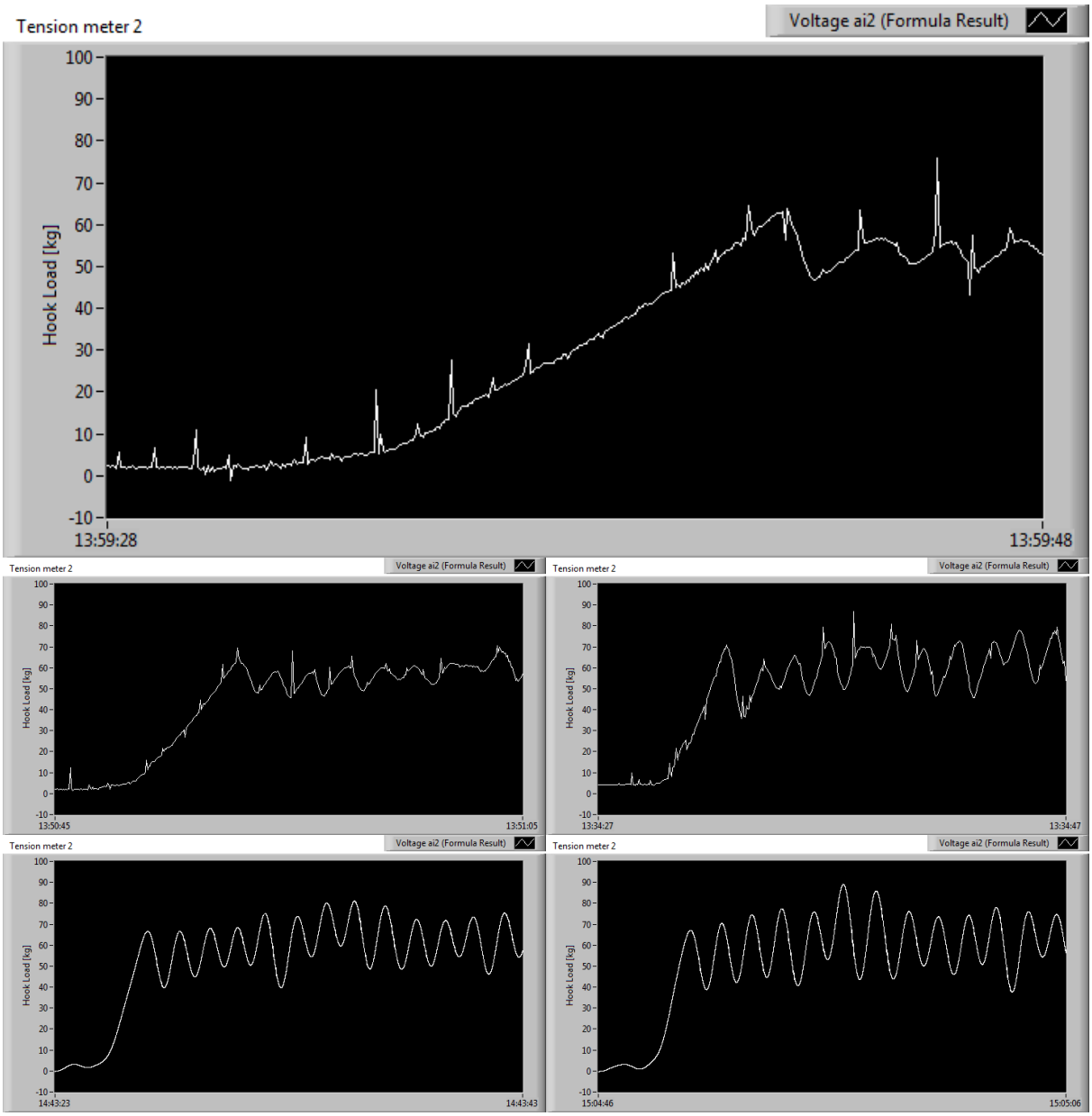

Figure 30: HKL on metal surface with medium low spring strength. Run velocity increasing from low to ultra high in the following order; top, center left, center right, lower left, lower right.

As seen in the charts, the HKL accelerated faster with higher velocity. The initial HKL peak increased slightly as the velocities increased. The wave behavior in the HKL was due to the elastic behavior in the drill string and the friction under the BHA. This was due to the changing friction factors going from static to dynamic state. The lower velocities had lower peaks after the initial peak, while the higher velocities had increasing peaks. That could have been due to the changing friction factor in the tray. The metal surface in the tray seemed to become smoother as more runs were performed on the metal surface. A lot of trial runs were performed before the experimental runs were performed, and the surface most exposed to the moving BHA was the upper part of the tray. Less runs went further down the tray. With higher velocities the BHA traveled further down, running over a rougher surface.

The peaks of the higher velocity runs were sharper than in the lower velocity runs. This was because of the increased accelerated force. Because the runs were faster they also created more peaks.

b) Metal Surface with Different Spring Strengths

Only the metal surface was tested with all the five springs. The charts in Figure 31 show the same velocity; high velocity. The figure shows the changes from the weakest spring strength to the strongest (see the different springs in Table 3).

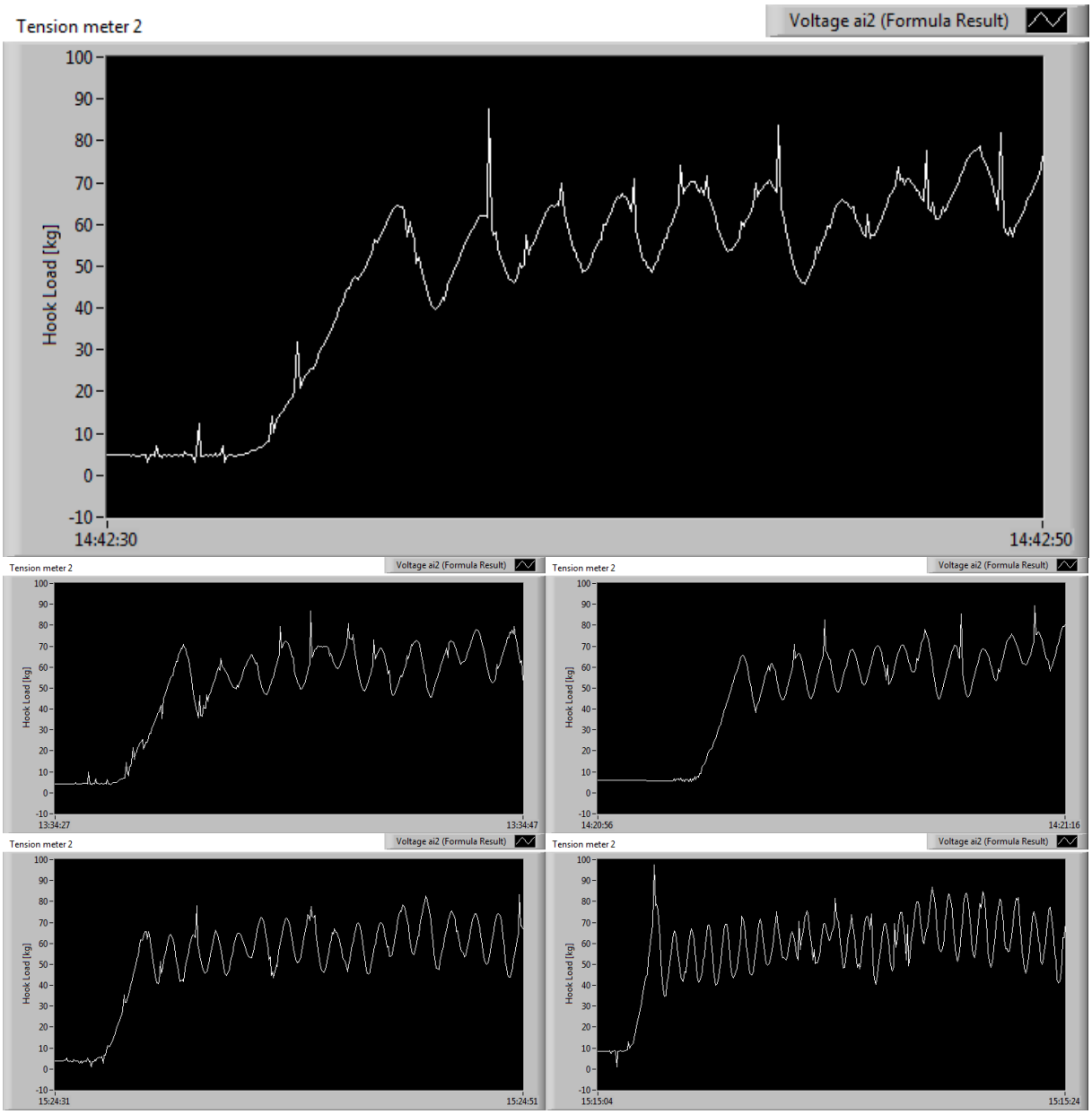

Figure 31: HKL on metal surface at high velocity. Spring strength increasing from low to high in the following order; top, center left, center right, lower left, lower right.

The stronger the springs were the less elasticity they had, and the faster the HKL increased. The stronger springs were shorter with less active coils, which made the springs less elastic. The runs with stronger springs reached the initial peak much faster and created sharper peaks. All of these runs were performed with the first custom designed program, so it was important to not confuse the spikes from the noise with the actual HKL. All the runs experienced an increasing HKL further down the tray even with different springs. As mentioned earlier, this was due to the change in the metal surface roughness.

c) Dry Sand Surface with Two Spring Strengths and Two Velocities

All the runs on cuttings were performed with the improved LabView program. The charts in Figure 32 show the runs on the dry sand surface. The two top charts show the medium low spring strength with low and high velocity, while the bottom charts show the high spring strength. The scale for the HKL increased up to 130 kg in the charts with cuttings.

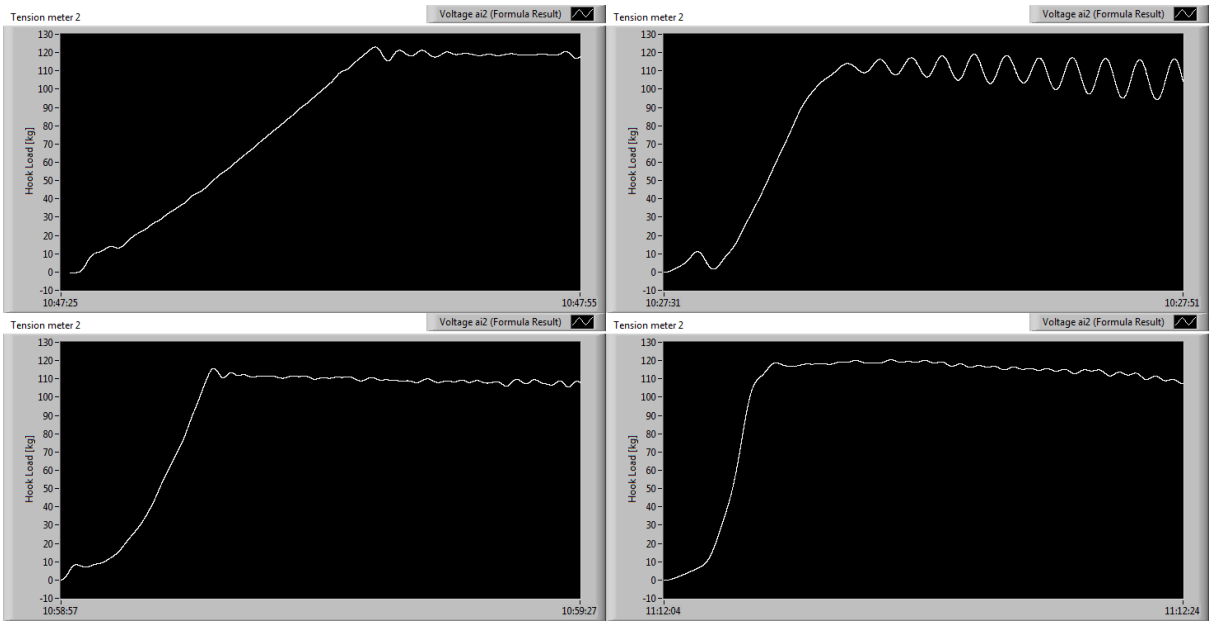

Figure 32: HKL on dry sand with two spring strengths and two velocities. The charts show the following: Medium low spring strength, low velocity (upper left) and high velocity (upper right); High spring strength, low velocity (lower left) and high velocity (lower right).

Tripping with the weaker spring created more oscillations because of elastic behavior, as seen in the top two charts. The longer the BHA was pulled the more of the sand surface underneath the BHA was plowed away. This made the BHA slide gradually more on the metal surface the further it traveled. The HKL with the strong spring increased much faster than with the weak spring, because of difference in elastic behavior. The low velocity runs did not have much oscillation. The reason they were so similar was because they did not run far enough to plow away the sand enough to slide on the metal surface.

The run in lower right chart with high speed also plowed away the sand. An initial peak was reached, but then the oscillation quickly stopped. This was because of the damping effect of the spring and the sand.

d) Water-Wet Sand Surface with Two Spring Strengths and Two Velocities

In Figure 33 the runs were performed with water and cuttings.

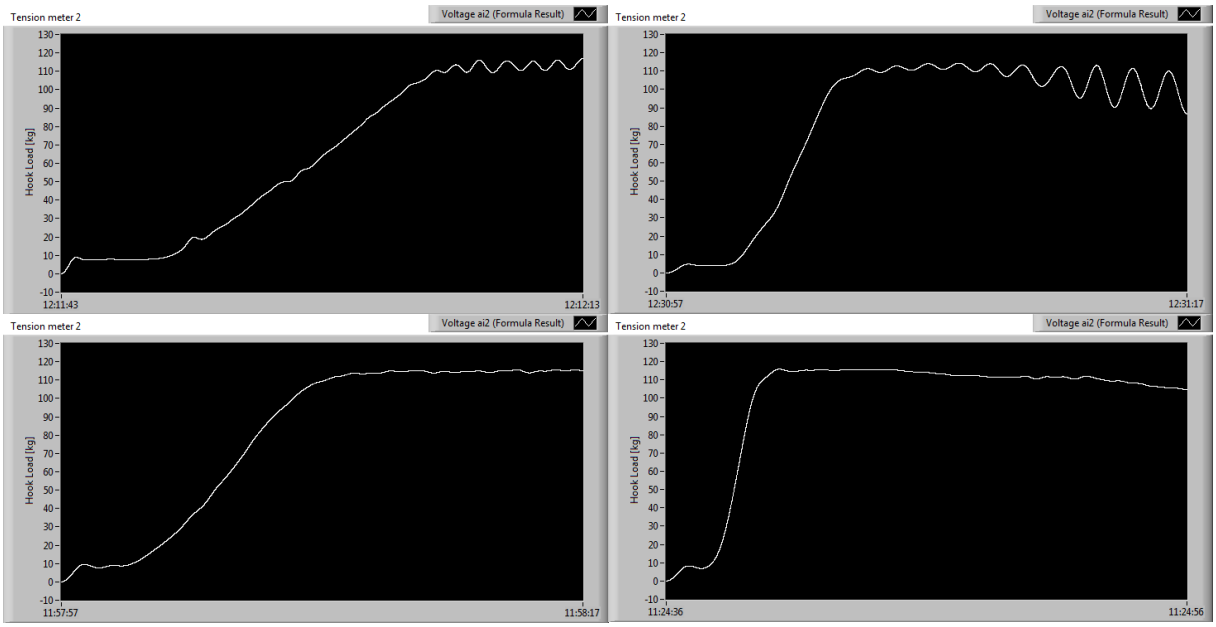

Figure 33: HKL on water-wet cuttings with two spring strengths and two velocities. The charts show the following: Medium low spring strength, low velocity (upper left) and high velocity (upper right); High spring strength, low velocity (lower left) and high velocity (lower right).

The HKL did not change much from the dry cuttings. The runs with the more elastic spring had more oscillation than with the less elastic spring, just as before. The HKL with the higher velocity and high spring strength decreased slightly with time. This was because the frictions coefficient of the metal surface was lower than the sand surface. As the sand was plowed away the HKL decreased.

e) Three Surfaces with Two Spring Strengths and Low Velocity

The charts in Figure 34 show the changes in HKL on the three different surfaces; metal, dry sand and water-wet sand. The medium low and high spring strengths were used. All the runs were performed at low velocity. The scale for the metal surface charts goes up to 100 kg, while the scale for the other charts goes up to 130 kg.

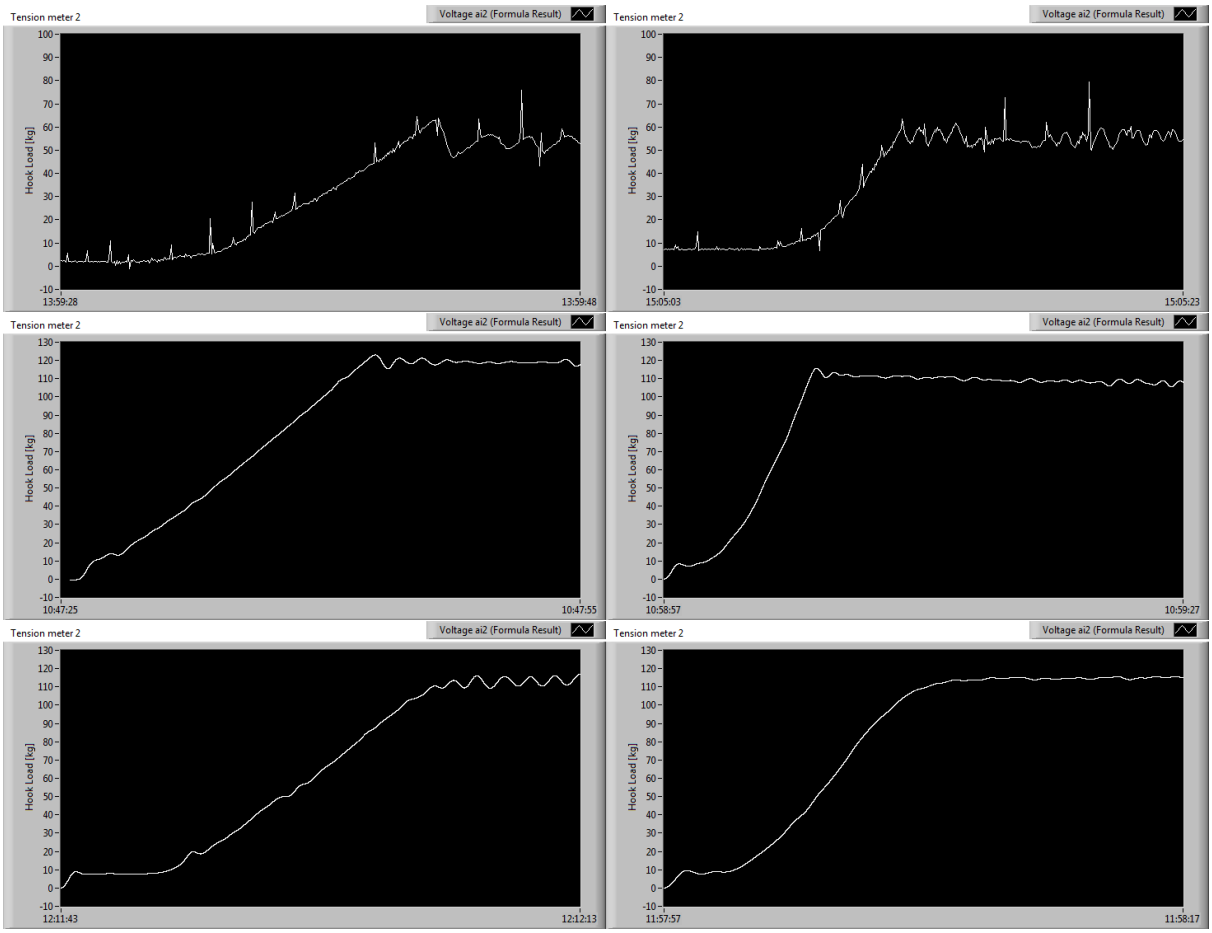

Figure 34: HKL on metal (upper charts), dry cuttings (center charts) and water-wet cuttings (lower charts). Both medium low spring strength (left charts) and high spring strength (right charts) ran with low velocity.

The HKL on sand increased from the metal surface to the cuttings. The HKL increased by approximately 50 kg. This shows that the friction factor on the cuttings was higher than on the metal. On cuttings the HKL did not drop much after the initial peak. The dynamic friction factor showed to be almost the same as the static friction factor. The run on dry cuttings experienced a higher initial peak than on the water-wet cuttings. The run on the water-wet cuttings also had smoother transition from static to dynamic state. This means that the friction factor for the dynamic state was higher than for the static state on water-wet cuttings.

Because the friction factors in static and dynamic state were so similar in cuttings, little to no potential energy was released from the extended springs, especially the strongest spring. That was the greatest reason why oscillations did not occur in those runs.

f) Three Surfaces with Two Spring Strengths and High Velocity

In Figure 35 the charts show the HKL on all the surfaces with the same spring strengths, but with high velocity.

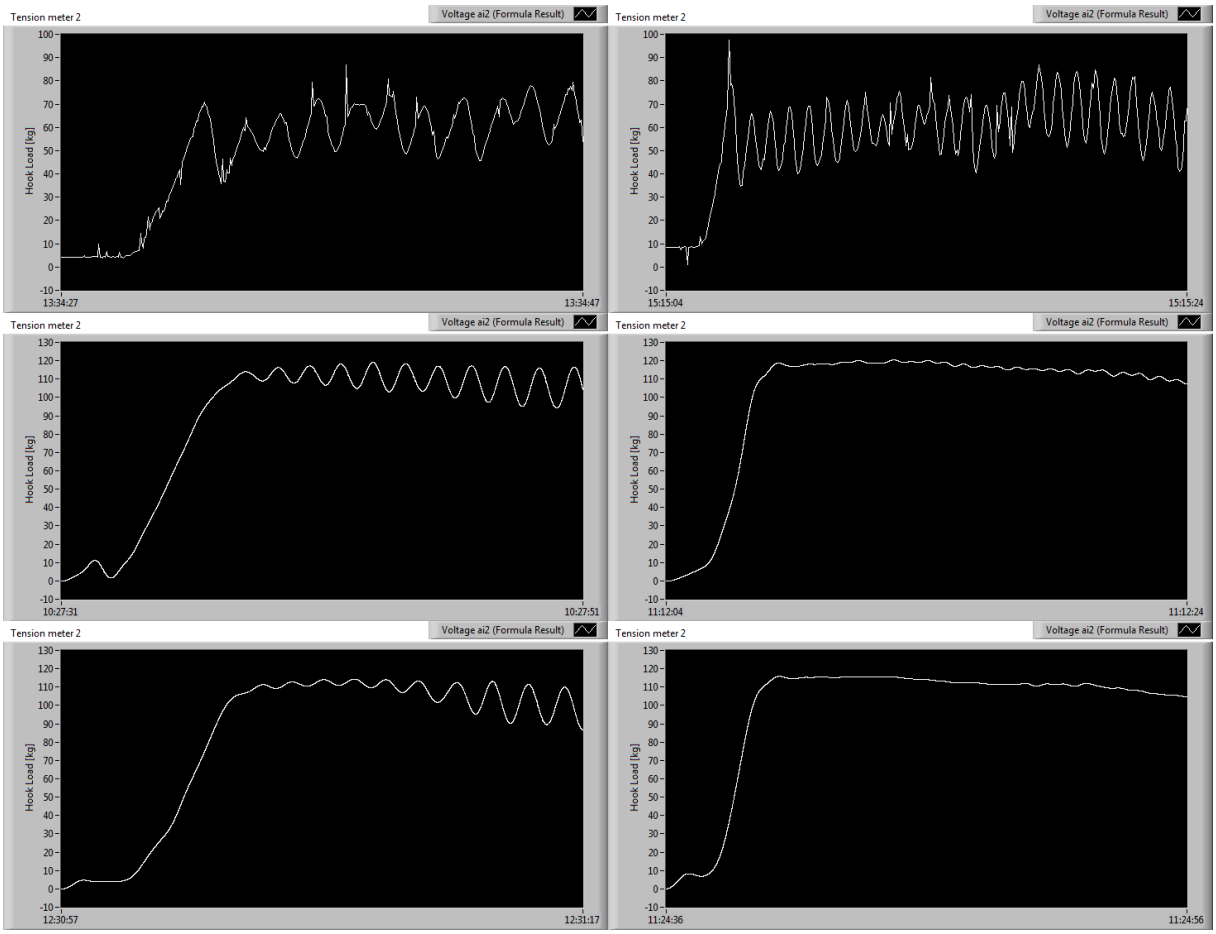

Figure 35: HKL on metal (upper charts), dry cuttings (center charts) and water-wet cuttings (lower charts). Both medium low spring strength (left charts) and high spring strength (right charts) ran with high velocity.

The HKL on water-wet cutting had even less oscillation than on dry cuttings.

With the lower spring strength the water kept the BHA from plowing down as fast as on dry cuttings. The greater oscillation on water-wet cuttings started later and was more gradual.

At high velocity the HKL did not oscillate with the stronger spring. The HKL experienced a small initial peak on both dry and wet cuttings with the strong spring. This questions the idea that the dynamic friction factor is higher than the static on wet cuttings. But the peak could be due to the increased acceleration. The HKL decreases over time on cuttings, best seen on the runs with little to no oscillation.

g) Velocity and Spring Strength Influence on Initial HKL

Different Frictions

The main focus of the results was the initial HKL peak. Figure 36 shows the difference in the HKL on three different surfaces; metal, cuttings and water-wet cuttings. The medium low and high spring strengths were utilized on all the surfaces.

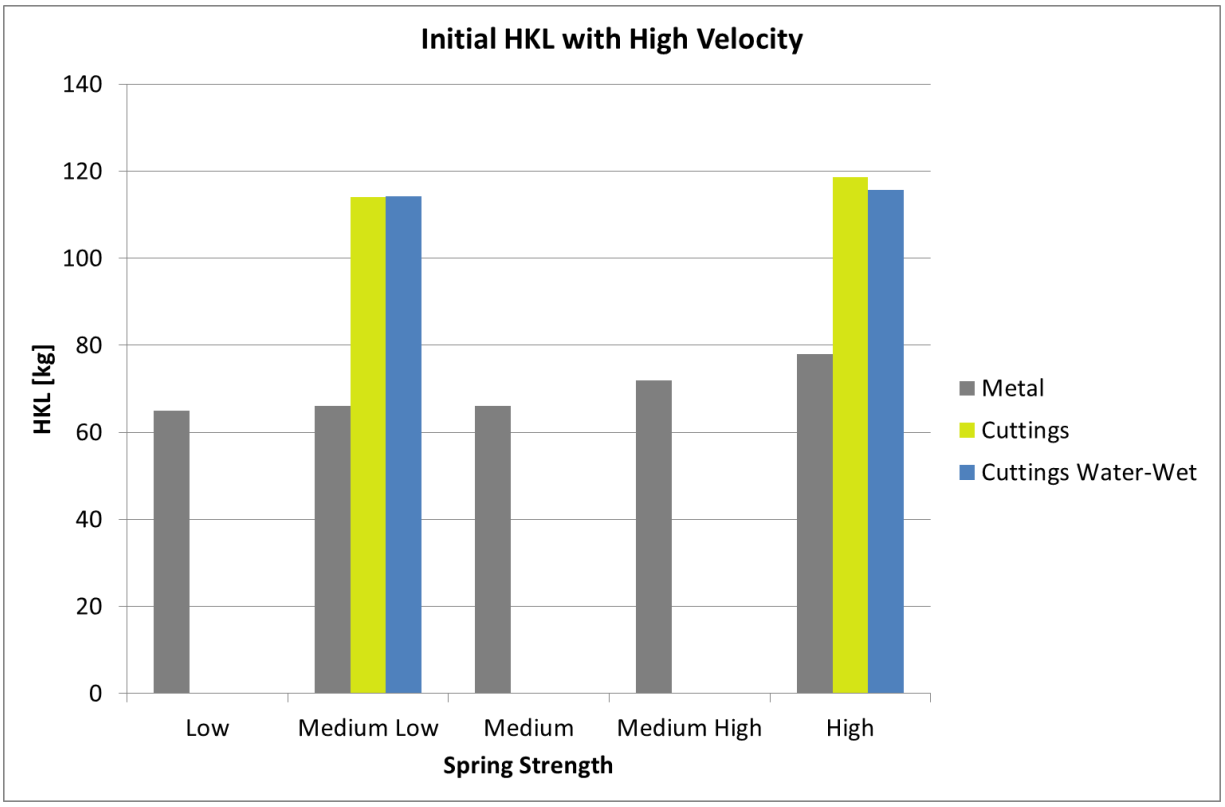

Figure 36: The stabilized "constant" HKL signal vs. type of friction and vs. spring strength at constant velocity (high)

The static friction factor was evidently greater on the cuttings bed than on the metal surface. The stabilized "constant" HKL also increased slightly with a less elastic drill string, probably due to a higher reactive force build up in the weak spring.

Pulling Velocity

The velocity of the drill string affected the initial HKL to a limited degree, as shown in Figure 37. The velocity can not affect the friction factor, but in the experiment it affected the acceleration of the BHA. The higher velocity runs only increased the HKL slightly.

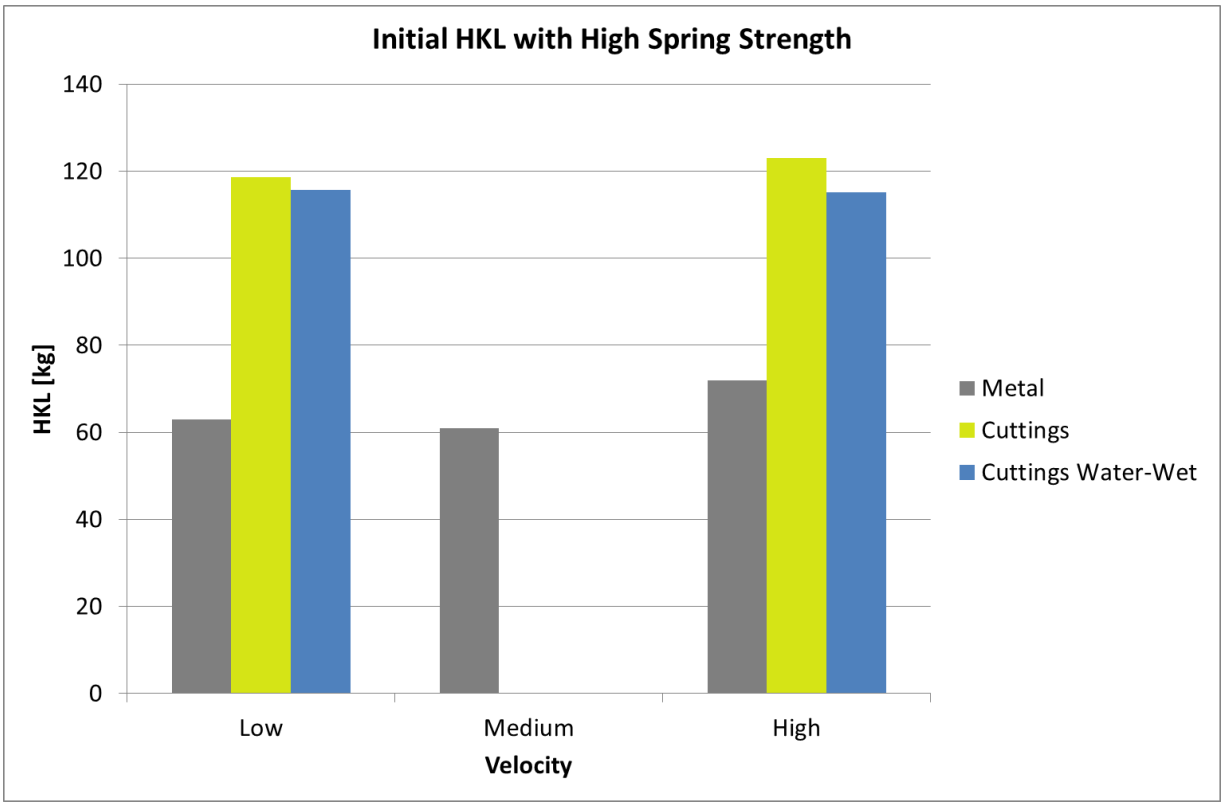

Figure 37: Initial HKL vs. velocity at constant spring strength (high)

The friction factor for the water-wet cuttings proved to be slightly smaller than on dry sand. The static friction factor for the surfaces can be calculated by using the initial HKL as following:

$$\mu_{static} = \frac{F_{HKL}}{F_N} \tag{28}$$

Table 9 shows a minimum and a maximum friction factor, because the HKL changed when the velocity and spring strength changed.

Table 9: Static Friction Factor vs. Type of Surface

Static Friction Factor	Surface		
	Metal	Cuttings	Cuttings Water-Wet
μ-min	0,255	0,485	0,486
μ-max	0,332	0,523	0,494

As shown in the results above, the velocity did not change the friction factor, and neither did the drill string elasticity. The actual static friction factor is then smaller than the minimum friction factor. This is also deduced from the following equations:

$$m \cdot a = k \cdot \Delta x - \mu \cdot m \cdot g \tag{29}$$

$$\mu = \frac{k \cdot \Delta x - m \cdot a}{m \cdot g} \tag{30}$$

h) Comparing Experimental Results with Field Data and Model

The results were finally compared to the field data from Figure 7 (Field Data One Stand Tripping Operations (Statoil, 2007)). The field data showed that the HKL increased rapidly, and once it surpassed the maximum static friction force the BHA started moving. The HKL in the dynamic state did not seem to change from the static state. The HKL also did not have any oscillating behavior. It was rather linear. The experimental runs that seemed to behave the most like the field data was the ones that ran on cuttings, wet and dry, with the high spring strength. The similarities could mean similar characteristics. This implies that the drill string had little elastic behavior, because if it was elastic, the HKL would most likely show more oscillation as seen in the experimental results with low spring strength (see Figure 34 and Figure 35). The static and dynamic friction factors seem to be very similar in the field data, as in the experiment.

The mathematical model with non-elastic behavior (see Figure 9 Matlab; Simple HKL Model of Experiment) showed some similarities to the field data and the experimental results. The field data did not show any initial peak, but the lab results did. But results showed that with a great initial peak, lots of peaks follow, and this is not shown in the model. The linear behavior in the dynamic state of the model was seen in both the field data and lab results. The lab results showed this when it ran on cuttings.

The mass-spring model did not have the data to simulate the experimental HKL, and was therefore just presented as an elastic model that could have modeled the initial HKL peak.

There are many uncertainties about the bore hole from the field data. What is certain is that the formation is very different from the metal surface in the experiment. The drill string could

have been on cuttings or just the naked formation, and the formation walls could have had static and dynamic friction factors that were approximately the same. The formation walls could also have been coated in fluids and filter cake that also affected the friction factor.

The friction factors seemed to be very high according to the project supervisor, even when considering that they are smaller than the minimum friction factors shown in Table 9 (Static Friction Factor vs. Type of Surface).

The main reason that the HKL oscillation is dampened in wells is due to the high friction along the drill string, especially in bends. Another reason is the hydraulic friction. The oscillations disappear on the way up. In a vertical well there are few damping affects.

7. Discussion

It was essential for the results that the experiments were well performed. This section discusses the quality of the model and the experiment.

7.1. Quality of the Model

The non-elastic model was created to simulate the initial HKL in a horizontal well during a tripping operation. The numerical models are always an approximation, trying to represent the real world. More components and complex factors could always be implemented into the model for improved accuracy. Due to the limited time of a master's thesis it is important to implement the most important elements, while excluding the less critical ones. Consequently, the model loses precision.

The non-elastic model is a simple model of Coulomb friction. It neglects a lot of key factors involved in the HKL. The HKL will, after reaching the peak, create an oscillation mode if there are no damping effects involved. In the experimental set up there were no damping elements involved.

Originally an elastic model was going to be designed to obtain a better understanding of the HKL. Certain information about the initial conditions was required to make such a model; information about the relative change in distance between the wire and BHA during the tripping respectively. This was realized first after the experiments were completed. The mass-spring model was presented as an example of an elastic model. This model includes circulation friction, buoyancy and multiple masses. The experiments were carried out with only one mass, the BHA, and no fluid circulation.

7.2. Quality of the Experiment

There were no faulty mechanics, wiring or programing from what was observed. The first assumption made was that the laboratory experiment did not have any faulty components. Many aspects to the experiments could have been improved. The experiment was only as good as the assumptions and boundaries dictate. The rig was made sturdy, robust and long lasting for future rigs.

The electrical wires were coiled up in order to reduce the noise interference in the signal readings. This limited somewhat the run distance of the BHA, because the electrical wire from TM200, right in front of the BHA, was moving away from the computer. The main reason for putting the tension meter right in front of the BHA was to avoid measuring the friction forces in the pulley system. If the tension meter was integrated in the dead line the friction forces in the pulley system would have been included in the HKL. Any other location for the tension meter would have made it further away from the computer, which meant less coiling of the wire.

The start of the HKL was inconsistent. There were two reasons for that; the amount of drill string wire that needed to be spooled in before the tension increased and the time difference between when the winch and the LabView program started. When the run started with a lot of slack in the wire the HKL had a delayed increase. If the recording in the LabView program started much later than the winch, the wire would already be in tension when the program started.

When the runs repeated themselves it was very important to recreate the same conditions every time. This was especially important when runs were performed on cuttings, because they were plowed away. When water was included the tray-surface had to be re-wetted every time. Every time the BHA was pulled back the cuttings were evened out with the same thickness and water was refilled. The runs were performed under the most consistent conditions to eliminate uncertainties.

The accuracy of the results also depended on the electrical wires, tension meters, dynamo, LabView etc. It was assumed that the equipment was in order and that it was working properly, since they were calibrated. The electrical wires could possibly have been faulty and sent poor signals. The tension meters and dynamo could possibly have sent irregular voltage signals. LabView could possibly have acquired the signals wrong, or the custom designed program could possibly have been faulty or poorly designed. All of these factors could have messed with the results. With limited resources and equipment assumptions were made; as long as the results looked reliable they were good.

The most important thing was how well the experiment could simulate field environment. If the results poorly simulated the field data, they could not be applied for tripping operations.

7.3. Future Work

The continued work on tripping operation is very important in order to prevent stuck pipe and damaged tools.

When the results were analysed it was assumed that the surface conditions were the same for each run. More runs could have been done under the same conditions to see if the results would repeat themselves or if they would change. If they repeated themselves enough it could mean that the runs gave a fairly accurate estimate. The non-performed runs could also have been performed for more data.

The noise could have been eliminated by giving the winch operating system new filters, putting a screen around it and relocating the position of the operating box.

One way of improving the plots could have been to integrate the winch and program buttons together. That way they would have started at the same time every time. By starting with a minimum tension every run, the slack wire problem could have been solved.

The field environment has a lot of elements that were not included in the simulation. That means the lab data could not perfectly simulate a true tripping operation. The results of the simulation can only be applied to the field when understanding its limitations.

To sum up, the further development of this work can be achieved by:

<u>Concerning the rig</u>

- Calculating the acceleration of the BHA
- Using different cuttings
- Adding mud to the surface of the BHA
- Creating a cylinder shaped BHA in a half pipe tray for better contact area
- Creating a surface with cuttings glued to the tray to better simulate rock formation walls
- Designing better draw works for a more stable wire
- Measuring the positions of the BHA and the wire on either side of the springs
- Suppressing or eliminating the source of the noise
- Creating a single stop button for both rig and program
- Including more variables for a more realistic tripping environment

Concerning the model

- Developing an elastic model that better represents the a tripping operation done in the experiment
- Measuring the velocity on either side of the springs
- Obtaining more measurements in the experiment to better develop a model

8. Conclusion

The following conclusions have been drawn based on the results, evaluation and discussion of this thesis:

- The HKL model was sacrificed to the focus on building and experimenting.
- A robust and strong HKL rig was successfully built.
- The testing and quality checking made certain problems apparent; noise, which was eliminated with better wiring and improved signal processing.
- The HKL signals looked promising and were approved for the experiment. The HKL signature resembled field data.
- The initial peak behavior occurred during every performed run.
- The friction factor proved to be independent of the velocity and drill string elasticity.
- The work on tripping needs further development by including more elements to better model and simulate the field environment.
- Furthering the work gives a better understanding of the problems during tripping, which can prevent or mitigate stuck pipe and damaged tools, which leads to NPT.

9. Nomenclature

α	inclination
β	buoyancy
Δ	initial distance between masses
ε	strain
θ	angle
μ	coefficient of friction, friction factor
μ_d	dynamic friction factor
μ_s	static friction factor
$\mu_{viscosity\ mud}$	mud viscosity
σ	stress
x	position of specific mass
Δx	spring length deformation
a	acceleration
A_{cs}	cross section area
c	rate
C_{sheave}	sheave circumference
d_h	diameter of hole
d_s	diameter of drill string
d_{sheave}	sheave diameter
D_t	wire diameter
D_y	outer diameter
E	Young' s modulus
F	force
F_0	initial force in Newton required force before the spring starts to extend
F_D	fluid drag force
F_{df}	dynamic friction force
F_{dl}	dynamic load

F_f	friction force
F_{max}	maximum permitted force for dynamic load in Newton
F_N	normal force
F_{sf}	static friction force
F_{sp}	spring force
F_W	force of drill string weight
g	gravity constant
k	spring konstant
L	length
L_0	free length
L_1	permitted extended length for dynamic load
ΔL	length of deformation
m	mass
m_{max}	maximum permitted force for dynamic load in kg
N	number of lines in hoisting system
n_v	number of active coils
t	time
V_{est}	estimated voltage
V_{output}	voltage output
v	velocity
v_{est}	estimated velocity
W	weight
W_A	angle weight
W_N	normal weight
X1	voltage input signal

BPOS	block position
CoF	coefficient of friction (friction factor)
ERD	extended reach drilling

HKL	hook load
ID	inner diameter
NFR	norges forskningsråd
NPT	non-productive time
NTNU	Norges teknisk-naturvitenskaplige universitet
OBM	oil based mud
OD	outer diameter
POOH	pull out of hole
RIH	run in hole
VI	virtual instrument
WBM	water based mud
WOB	weight on bit

10.References

AADNOY, B. S., FAZAELIZADEH, M. & HARELAND, G. 2010. A 3D Analytical Model for Wellbore Friction.

BJERKE, H. 2013. *Revealing Causes of Restrictions by Signatures in Real-Time Hook Load Signals.* Master's Degree, Norwegian University of Science and Technology.

CORDOSO, J. V., JR., MAIDLA, E. E. & IDAGAWA, L. S. 1995. Problem Detection During Tripping Operations in Horizontal and Directional Wells.

ENGINEERING, O. G. D. 2015. *Drilling Rig Hoisting System* [Online]. Available: http://www.oilngasdrilling.com/drilling-rig-hoisting-system.html [Accessed May 2015].

GLOMSTAD, T. S. 2012. *Analysis of Hook Load Signal to Reaveal the Causes of Restriction.* Master's Degree, Norwegian University of Science and Technology.

KRISTENSEN, E. 2013. *Model of Hook Load During Tripping Operation.* Master's Degree, Norwegian University of Science and Technology.

LUKE, G. R. & JUVKAM-WOLD, H. C. 1993. The Determination of True Hook-and-Line Tension Under Dynamic Conditions.

MAIDLA, E. E. & WOJTANOWICZ, A. K. 1990. Laboratory Study of Borehole Friction Factor With a Dynamic-Filtration Apparatus.

MME, U., SKALLE, P., JOHANSEN, S.T ET AL. 2012. Analysis and modeling of normal hook load response during tripping operations.: Norwegian University og Science and Technology.

PETROWIKI. 2013. Glosary: Hook Load [Online]. Available: http://petrowiki.org/Glossary%3AHook_load [Accessed May 2015].

SJØBREND, A. 2014. Building, Testing and Qualifying New Hook Load Rig. Master's Degree, Norwegian University of Science and Technology.

STATOIL 2007. Drilling and Completion 34/10-C-47. Statoil.

WIKIPEDIA. 2015. Friction [Online]. Available: http://en.wikipedia.org/wiki/Friction#Limitations_of_the_Coulomb_model [Accessed May 5 2015].

11.Appendix